Authors' response to the Editor and the Referees

Dear Editor, dear Referees,

We thank you for your time reviewing the manuscript and for your constructive comments and suggestions for improving the manuscript.

We have addressed all of the comments addressed in the reviews. Please find below a point-by-point response to the Review Reports as well as a marked-up manuscript version.

We await your decision on this revised version of the manuscript, and please contact us in case you require any additional information or clarification.

On behalf of all authors,

Sincerely,

Verner B. Ernstsen
Associate Professor
Department of Geosciences and Natural Resource Management
University of Copenhagen, Denmark

Authors' response to Report #2 of Referee #1

Authors' response is italicized.

R1: The authors have done an excellent work in revising this manuscript based on the comments from the three reviewers. Most of my earlier concerns have been addressed by the authors in this revised version. The manuscript is now situated in context, with appropriate referencing, and the novelty is clearer. The discussion is better and the application (morphological characterization) makes it a more complete paper, suitable for publication in HESS. I only have a few comments listed below that I am sure the authors will be able to address.

R1: 1. I would suggest reducing the length of the title, for instance by removing "in the coastal zone" since the mention of "high-energy tidal environment" already suggests that it is in a coastal environment.

The length of the title has been reduced as suggested.

R1: 2. In the abstract (p. 1 line 17), I would replace the word "harsh" by either "difficult" or "challenging". I feel like these have a different meaning and environmental conditions are not necessarily harsh, but can be challenging for surveying. The authors use "challenging" to describe them in the main text, and the abstract should be consistent with the main text.

The adjectives describing the environmental conditions have been changed as suggested.

R1: 3. As noted in the previous round of reviews, I recommend not using digital elevation model (DEM) when considering both elevation and depth like in this study. Since the data include cottages and vegetation, I believe that the most appropriate term would be Digital Surface Model (DSM), as opposed to Digital Terrain Model (DTM) that represents a "bare-earth" model.

We acknowledge the point that the elevation model includes cottages and vegetation, hence it could be called a DSM. However, after many considerations we have decided to maintain the term DEM, because this study generally focuses on the terrain/morphology, hence DSM will not be the appropriate term to use in this context. Only one figure visualizes the cottages and vegetation in the northern part on Fanø, and this part is not used in the geomorphometric and morphological analysis and classification. Obviously, DTM would be an incorrect term due to the cottages and vegetation, and therefore we have settled on the broader DEM term, which we find to encompass all the different environments in the elevation model.

Regarding the use of "elevation" for topography and bathymetry, we have investigated the issue and we are confident that it can be used with positive values above sea level and negative values below, e.g. ESRI defines "elevation" as:

"The vertical distance of a point or object above or below a reference surface or datum (generally mean sea level)"

(http://support.esri.com/other-resources/gis-dictionary/search/elevation)

In comparison they define "altitude" as:

"The height or vertical elevation of a point above a reference surface. Altitude measurements are usually based on a given reference datum, such as mean sea level"

(http://support.esri.com/other-resources/gis-dictionary/search/altitude)

We also found that "DEM" is an often used term for bathymetric or topobathymetric elevation models in the published literature (Chust et al., 2010; Coleman et al., 2011; Fernandez-Diaz et al., 2014; Finkl et al., 2005; Galparsoro et al., 2013; Pe'eri and Long, 2011; Wedding et al., 2008).

Based on the arguments above, we decided to keep the DEM-term, and to replace "altitude" with "elevation" throughout the text.

R1: 4. Also noted before: “landscape” has different meanings depending on the field of study (e.g. in landscape ecology or remote sensing). I recommend removing the two instances on page 17 and replacing them by “terrain”.

Landscape has been changed to terrain as suggested.

R1: 5. Another one noted before: change “small-scale” and “large-scale” for “fine-scale” and “broad-scale” throughout the text and in figures (e.g. Fig. 4). The formers have different meanings in cartography and other fields than in this study. The latters are less ambiguous.

Small- and large-scale have been changed to fine- and broad-scale throughout the manuscript as suggested.

R1: 6. On page 8 (lines 3 to 14), this should be moved to the methods section below, likely between lines 19 and 20 of that same page. At line 9, I would change the first “surface” for a word like “top” to make it clearer, e.g. “…located in the river with its top just below the water surface.”

Corrections have been done as suggested.

R1: 7. I understand how the method that is described in this manuscript is more transparent, reproducible and user-friendly than current alternatives. However, I am unsure of the level of reproducibility for two reasons. First, while the authors use RiHYDRO, HydroFusion and LiDAR Survey Studio as examples for describing the lack of transparency in available software (p. 6), the proposed method still requires many software that may not be widely available for all users and are not necessarily more transparent (e.g. RiPROCESS, HydroVish, Fledermaus, MATLAB). Second, many steps involve manual processing (e.g. filtering, extracting the shallow surface) or subjective decisions (e.g. parameters for automatic filtering, classification trees, values of 4 for standard deviation to differentiate between features). I appreciate that the authors mention these limitations (e.g. p. 11 and 28), however I believe that care should be used when making claims like at page 22 (“it is open to the public”), especially since the software used may not be accessible to the public. I wouldn’t go as far as suggesting the removal of mentions of “reproducible”, but I would be curious to see if this issue will also be of concern to other reviewers or the editor.

We acknowledge the point that we use software which is not accessible to the public; however, when using these software we describe how they work so there is no “black box”. In this way the processing method is not software specific. In principle our method could be reproduced in other software packages, or one could develop own software using the proposed method. Therefore, we have changed the phrasing “open to the public”, but we have not removed mentions of “reproducibility”.

R1: 8. On page 13, line 11, what do the authors mean by “only taking the top 95-100% of water points into account”? If 100% of the points are considered, then they are all accounted for and can’t possibly increase reliability. Please clarify.

We agree. It should be 1-5%. We have changed this accordingly.

R1: 9. On page 13, lines 16 to 31 are confusing. I am unsure what is the relationship between the 2 x 2 m water surface and the 0.5 x 0.5 m surface. I understand that the 2 x 2 m was built to remove outliers, but what is it used for then? This section requires rewording or clarifications.

We have rephrased this section in order to clarify the use of a 2 x 2 m and a 0.5 x 0.5 m grid, respectively.

R1: 10. On pages 16 and 17, please specify what the standard deviation represents (for the BPI). Is it the standard deviation of depth/elevation values within the window of analysis?

Yes, it is the STD of the altitude within the window of analysis. We have rephrased the paragraph to clarify this.

R1: 11. On page 17 (lines 3-4), I do not understand what the authors mean by "the altitude was exaggerated 10 times before the classification, to enable the BTM to detect the shapes of the landscapes". A vertical exaggeration in the visual representation of data would not change the altitude (depth or elevation) values and thus would not impact the results. If this is the case, then this sentence is unnecessary and can be removed. However, if the altitude values were actually altered and multiplied by a factor of 10, I am not sure if the analysis is still valid, although it would likely not change the relative values of pixels and still identify peaks and pits (but maybe reduce the amount of flat areas?). This needs to be clarified.

The actual values of the altitude were exaggerated by a factor of 10 because without exaggeration the BTM-tool did not show meaningful results with respect to the classification of crests and depressions. We have rephrased the paragraph to clarify this. We believe that it is still a valid analysis because the relative difference between cell values has not been changed. When it comes to slopes and flats, the input parameter was the slope of the actual altitudes (not the exaggerated), so the amount of flat areas is not affected by the exaggeration.

R1: 12. Page 17, line 5: "the best results" based on what? Visual interpretation? Was it a subjective decision? Please specify.

Yes, it was based on visual interpretation. We have clarified this.

R1: 13. In Figure 5 and associated text, is everything >0.94 m really a beach dune? Weren't there cottages and other features? Would another term be more appropriate and all-encompassing of features that were above the water level?

We are generally focusing on the natural environment, and therefore, we have excluded the northern part with cottages in the classification analyses. This is now clarified in the paper. Besides, Beach Dunes are not only > 0.94 m: The DEM also has to be 0.8 m above the "smooth DEM" as shown in Figure 5.

R1: 14. On page 18, I believe that the window sizes are wrong. They would only make sense if a radius was used instead of a window of analysis. Window sizes need to be odd numbers and based on the pixel size (0.5 m), the window could not be of 100 m or 250 m wide. Please revise these measurements, indicate whether a window of analysis (square) was used or a radius (circle), and whether these numbers are the numbers of pixels of the window or the actual area covered by the window (in either cases it should be an odd number).

You are absolutely right! We actually used 99.5 m and 249.5 m in square windows in the analysis, but we presented these as round numbers, i.e. 100 m and 250 m, to make it more comprehendible for the reader. We have now also added the exact numbers.

R1: 15. For your information, standard deviation (cf. classification trees) is used as a measure of rugosity in geomorphometry, so when the authors used it to distinguish between bars and larger features, they used a measure of broad-scale rugosity.

Yes, you are absolutely right, thanks. Rugosity is to some extent a "problematic" term, as it is defined and quantified differently in different disciplines, like the case of landscape.

R1: 16. Page 18, lines 29-30: "4 were found to be a suitable ratio threshold". Based on what (e.g. visual interpretation, etc.)?

Yes it was based on visual interpretation. We have clarified this.

R1: 17. In Figure 10 (B-C-D), I would add a category in the legend to characterize the grey areas (that I assume are no data, i.e. the areas that did not correspond to any of the criteria in the decision/classification tree). This category could be named "Transition zones".

We have termed this category "Unclassified".

R1: 18. On page 25, lines 4 to 17 are repetitive to the methods section (p. 9). I would bring back the description of the environmental conditions at time of survey in the methods section, and keep the discussion on their implications at p. 25.

Rearrangements have been made as suggested.

R1: 19. The use of English language could be improved before publication, although it is not a big concern at the moment as the text remains clear. For instance, p. 10 line 21 should read “Steps 5-8 represent” instead or “Step 5-8 represents”, p. 12 line 14 “currently” should be removed since it was at time of survey, p. 18 line 29 “was” instead of “were”, p. 29 line 18 “are” instead of “is”, etc.. These are only a few examples of where corrections should be made. Also, in some parts of the text that describe the methods and results, the past tense should be used.

Thanks for your specific suggestions; additionally, we have improved the language, including the issues related to past and present tense.

References

Chust, G., Grande, M., Galparsoro, I., Uriarte, A., and Borja, Á.: Capabilities of the bathymetric Hawk Eye LiDAR for coastal habitat mapping: A case study within a Basque estuary, Estuarine, Coastal and Shelf Science, 89, 200-213, 2010.

Coleman, J. B., Yao, X., Jordan, T. R., and Madden, M.: Holes in the ocean: Filling voids in bathymetric lidar data, Computers & Geosciences, 37, 474-484, 2011.

Fernandez-Diaz, J. C., Glennie, C. L., Carter, W. E., Shrestha, R. L., Sartori, M. P., Singhania, A., Legleiter, C. J., and Overstreet, B. T.: Early Results of Simultaneous Terrain and Shallow Water Bathymetry Mapping Using a Single-Wavelength Airborne LiDAR Sensor, IEEE J. Sel. Top. Appl. Earth Observations and Remote Sens., 7, 623-635, 10.1109/JSTARS.2013.2265255, 2014.

Finkl, C. W., Benedet, L., and Andrews, J. L.: Interpretation of seabed geomorphology based on spatial analysis of high-density airborne laser bathymetry, Journal of Coastal Research, 501-514, 2005.

Galparsoro, I., Borja, Á., Kostylev, V. E., Rodríguez, J. G., Pascual, M., and Muxika, I.: A process-driven sedimentary habitat modelling approach, explaining seafloor integrity and biodiversity assessment within the European Marine Strategy Framework Directive, Estuarine, Coastal and Shelf Science, 131, 194-205, 2013.

Pe'eri, S., and Long, B.: LIDAR technology applied in coastal studies and management, J Coastal Res, 1-5, 2011.

Wedding, L. M., Friedlander, A. M., McGranaghan, M., Yost, R. S., and Monaco, M. E.: Using bathymetric lidar to define nearshore benthic habitat complexity: Implications for management of reef fish assemblages in Hawaii, Remote Sensing of Environment, 112, 4159-4165, 2008.

Authors' response to Report #1 of Referee #2

Authors' response is italicized.

R2: The authors had made adequate revisions and the quality has been improved largely. However, there are still some aspects to improve.

R2: 1. The research content is abundant, which can be divided into two papers: one for Processing and performance of topobathymetric LiDAR data, the other one for geomorphometric and morphological classification. Because of the abundant content, the aim of this research is difficult to focus.

> *Our original idea was, as you have suggested, dividing our study into two papers, which is why the paper at the first submission included only the Processing and performance of topobathymetric LiDAR. However; the first round of reviews, and complimented by the Editor, highlighted the necessity of including a morphological quantitative analysis in order to place the technical part of the study in context and to demonstrate the application of the topobathymetric LiDAR data. We acknowledged this; and in our response to the first round of reviews we stated how we would approach this, which was then realised by adding the geomorphometric and morphological analysis in the revised manuscript. In retrospect we truly agree with the referee in review report 2 of the second round of reviews that the application (i.e. the morphological characterization) makes it a more complete paper. Moreover, we believe that it is very valuable to present the complete processing line from raw topobathymetric LiDAR data to automatic landform classification based on geomorphometric analyses. Finally, we sincerely believe that we have developed novel methods for processing green LiDAR data and for classifying morphological units in coastal tidal environments using geomorphometry.*

R2: 2. The presentation can be improved in some aspects. For example, the "introduction" section is too long, and Page 4 can be placed into "methodology" section. In addition, Section 3.2 can be made into a diagram.

> *We have aimed at improving the presentation of the study and its findings: We have shortened the introduction section; this includes moving the description of topobathymetric LiDAR to the methods section as suggested. Section 3.2 is already visualized in the quite comprehensive Figure 3, which functions both as a flow diagram of the processing steps as well as a visualization of the individual processing steps. So we believe the referee suggestion has been acknowledged in the paper.*

R2: 3. Because of abundant content, the figures is too much.

> *We acknowledge that the number of figures may seem relatively high but we find the figures relevant to aid the reader and to convey our findings. However, we suggest excluding Fig. 12, which shows the spatial coverage of the dead-zone at different water levels. We have removed this figure from the paper and made the required changes in the text.*

R2: 4. The geomorphometric classification is not mentioned in the "conclusion" section.

> *The results of the geomorphometric classification were not included in the conclusions, as this was considered a step on the way towards the final morphological classification. However, we truly acknowledge that the geomorphometric classification constitutes one of the central parts of the study; hence we have included it in the conclusions as suggested.*

R2: Overall, I do not think one paper should put so many issues. I suggest the authors can focus on one or two issues and illustrate deeply and concisely.

> *Please refer to the history of the paper outlined under point 1.*

Processing and performance of topobathymetric LiDAR data for geomorphometric and morphological classification in a high-energy tidal environment in the coastal zone

M.S. Andersen[1], Á. Gergely[1], Z. Al-Hamdani[2], F. Steinbacher[3], L.R. Larsen[4], V. B. Ernstsen[1]

[1] Department of Geosciences and Natural Resource Management, University of Copenhagen, Denmark

[2] Geological Survey of Denmark and Greenland, Denmark

[3] Airborne Hydro Mapping GmbH, Austria

[4] NIRAS, Denmark

Correspondence to: V. B. Ernstsen (vbe@ign.ku.dk)

Abstract

The transition zone between land and water is difficult to map with conventional geophysical systems due to shallow water depth and often harshchallenging environmental conditions. The emerging technology of airborne topobathymetric Light Detection And Ranging (LiDAR) is capable of providing both topographic and bathymetric elevation information, using only a single green laser, resulting in a seamless coverage of the land-water transition zone. However, there is no transparent and reproducible method for processing green topobathymetric LiDAR data into a Digital Elevation Model (DEM). The general processing steps involve data filtering, water surface detection and refraction correction. Specifically, the procedure of water surface detection and modelling, solely using green laser LiDAR data, has not previously been described in detail for tidal environments. The aim of this study was to fill this gap of knowledge by developing a step-by-step procedure for modelling the water surfacemaking a Digital Water Surface Model (DWSM) using the green laser

LiDAR data. The detailed description of the processing ~~method~~procedure augments its reliability, makes it user friendly and repeatable. A DEM was obtained from the processed topobathymetric LiDAR data collected in spring 2014 from the Knudedyb tidal inlet system in the Danish Wadden Sea. The vertical accuracy of the LiDAR data is determined to ±8 cm at a 95% confidence level, and the horizontal accuracy is determined as the mean error to ±10 cm. The LiDAR technique is found capable of detecting features with a size of less than 1 m^2. The derived high resolution DEM was applied for detection and classification of geomorphometric and morphological features ~~in~~within the natural environment of the study area. Initially, the Bathymetric Positioning Index (BPI) and the slope of the DEM were used to make a continuous classification of the geomorphometry. Subsequently, stage (or elevation in relation to tidal range) ~~was used to divide the area of investigation into the different tidal zones, i.e. subtidal, intertidal and supratidal. Subsequently,~~ and a combination of statistical neighbourhood analyses (~~Bathymetric Positioning Index,~~ moving average and standard deviation) with varying window sizes, combined with the ~~first derivative slope and the area/perimeter-ratio~~DEM slope were used to ~~identify and characterise morphometric units. Finally, these morphometric units were classified~~ classify the study area into six ~~different~~specific types of morphological features (i.e. subtidal channel, intertidal flat, intertidal creek, linear bar, swash bar and beach dune). The developed classification method is adapted and applied to a specific case, but it can also be ~~transferred to~~implemented in other cases and environments.

1 Introduction

The coastal zone is under pressure from human exploitation in many and various ways. Many large cities are located near the coast, and they grow gradually with the increase in worldwide population and urbanization. Many industrial activities take place in close vicinity to the coast, e.g. fishery, construction, maintenance dredging for safety of navigation, and mining for raw materials. The coastal zone also provides the setting for many recreational and touristic activities, such as sailing, swimming, hiking, diving and surfing. In addition to human exploitation, climate change also poses a future threat with a predicted rising sea level and increasing storm intensity and frequency, expected to cause erosion and flooding in the coastal zone (Mousavi et al., 2011). All these pressures and different interests underpin the societal need for high resolution mapping, monitoring, and ~~sustainably managing of~~sustainable management in the coastal zone.

~~The~~Historically, the transition zones between land and water have been difficult or even impossible to map and investigate in high spatial resolution due to the difficulties in collecting data in these challenging~~ environmental conditions,~~ high-energy environments. The airborne near-infrared (NIR) Light Detection ~~and ~~And Ranging (LiDAR) is a technique often used for measuring high-resolution topography, however, NIR laser is incapable of measuring bathymetry due to the absorption and reflection of the laser light at the water surface. Traditionally, high-resolution bathymetry is measured with a multibeam echosounder (MBES) system mounted on a vessel, but it does not cover the bathymetry in the shallow water due to the vessel draft limitation.

NIR LiDAR and MBES are applied in different environments; however, the data are very similar and the processed high-resolution topography/bathymetry ~~are both~~is often captured, visualised and analysed in a Digital Elevation Model (DEM). The processed DEM may be applied for various purposes, e.g. for geomorphological mapping. Previous studies classifying morphology in either terrestrial or marine environments have been performed numerous times (Al-Hamdani et al., 2008; Cavalli and Marchi, 2008; Hogg et al., 2016; Höfle and Rutzinger, 2011; Ismail et al., 2015; Kaskela et al., 2012; Lecours et al., 2016; Sacchetti et al., 2011). These classification studies generally focus on either the marine or the terrestrial environment~~,~~ and ~~they ~~do not cover the ~~small~~fine-scale morphology in the shallow water~~ at the land-water transition zones~~, due to the ~~challenges of collecting data in these high-energy environments. A~~challenging environmental conditions. To overcome this impediment a new generation of airborne green topobathymetric LiDAR that enables high resolution measurements of both topography and shallow bathymetry~~, and for that reason it is specifically suited to map the land-water transition zone~~ has been introduced (Guenther, 1985; Jensen, 2009; Pe'eri and Long, 2011). The potential of merging morphological classifications of marine and terrestrial environments enables a holistic approach for managing the coastal zone.

~~Topobathymetric LiDAR is based on continuous measurements of the distance between an airplane and the ground/seabed. The distance (or range) is calculated by half the~~

travel time of a laser beam, going from the airplane to the surface of the earth and back to the airplane. The wavelength of the laser beam is in the green spectrum, usually 532 nm, since this wavelength is found to attenuate the least in the water column, resulting in the largest penetration depth of the laser (Jensen, 2009). In literature, The raw topobathymetric LiDAR data is sometimes referred to as either bathymetric LiDAR or Airborne LiDAR bathymetry (ALB). These are just different terms with the same meaning, and in this paper, topobathymetric LiDAR is preferred, since it describes the system's ability to simultaneously measure bathymetry as well as topography.

A single laser beam may encounter many targets of varying nature on its way from the airplane and back again, and different processes are influencing the laser beam propagation through air and water. First, the laser beam may be reflected by targets in the air, such as birds or dust particles, and these can show up as LiDAR reflection points in the space between the airplane and the surface. When encountering water, the speed of the laser decreases from 3×10^8 ms^{-1} to e.g. 2.25×10^8 ms^{-1} in 10°C freshwater or e.g. 2.24×10^8 ms^{-1} in 10°C saltwater of 30 PSU (Millard and Seaver, 1990).

The changing speed of the laser beam also affects the direction of the laser beam when penetrating the water surface with an angle different from nadir (Fig. 1) (Guenther, 2007; Jensen, 2009). The laser beam will be refracted according to Snell's Law (Mandlburger et al., 2013):

$$\frac{\sin\alpha_{air}}{\sin\alpha_{water}} = \frac{c_{air}}{c_{water}} = \frac{n_{water}}{n_{air}} \qquad (1)$$

where α_{air} is the incidence angle of the laser beam relative to the normal vector of the water surface and α_{water} is the refraction angle in water. n_{water} and n_{air} are the refractive indices of water and air, respectively (Mandlburger et al., 2013).

The penetration depth in water is limited by the attenuation of the laser beam. Water molecules, suspended sediment and dissolved material all act on the laser beam by absorption and scattering, resulting in substantial reduction in power as the signal propagates into the water (Guenther, 2007; Mandlburger et al., 2013; Steinbacher et al., 2012). The laser beam also diverges in the water column, resulting in a wider laser beam footprint (Guenther et al., 2000), and this effect reduces the resolving capability of fine-scale morphology the deeper the laser beam penetrates.

~~The returned signal is represented as a distribution of energy over time, also called the 'full waveform' (Alexander, 2010; Chauve et al., 2007; Mallet and Bretar, 2009). The peaks in the full-waveform are detected as individual targets encountered by the propagating laser beam. If the laser hits two targets with a small vertical difference, such as a water surface and seabed in very shallow water, then the two peaks in the full-waveform may merge together, resulting in the detection of only one target (Fig. 1). This results in a detection minimum of successive returns from a single laser pulse, and the vertical distance within this minimum is referred to as the 'dead zone' (Mandlburger et al., 2011; Nayegandhi et al., 2009). The dead zone is a clear limitation to the LiDAR measurements, which is an important parameter to consider in very shallow water, such as intertidal environments.~~

~~The raw LiDAR~~The raw topobathymetric LiDAR measurements are spatially visualized as points in a point cloud, with each point ~~representing an individual target.~~containing information of its location and elevation. The point cloud must be piped through a series of steps before it can ~~take shape~~be visualised as a DEM. Most of the processing steps required to process raw topobathymetric LiDAR data ~~to~~into a DEM are similar to the processing steps of topographic LiDAR data (Huising and Gomes Pereira, 1998). However, additional processing steps are required for topobathymetric LiDAR data due to the refraction of the laser beam at the water surface. All submerged LiDAR points have to be corrected for ~~the~~ refraction~~, but in order to do so~~; therefore, the water depth must be known for each point. This sets a requirement ~~of modelling the water surface~~for making a Digital Water Surface Model (DWSM), before the refraction correction can be performed. ~~The general processing procedure is well defined; however, there is no standard or universal approach for how to deal with these steps. LiDAR companies have their workflows, but the specific steps in their workflow are usually hidden, which make them non-repeatable.~~

~~In particular, there is no definitive method for detecting a water surface from green topobathymetric LiDAR data.~~ Often the water surface is detected and modelled from simultaneous collection of green and NIR LiDAR measurements, where the green laser reflects from the seabed and the NIR laser reflects from the air-water interface, and the NIR laser data are then used to detect and model the water surface (Allouis et al., 2010; Collin et al., 2008; Guenther, 2007; Parker and Sinclair, 2012). The use of NIR LiDAR data for water surface detection has been applied in several studies. For instance, (Hofle et al. (2009)) proposed a method for mapping water surfaces based on the geometrical and intensity information from NIR LiDAR data. ~~Su and Gibeaut (2009) classified water points from NIR LiDAR based on point density, intensity and altitude.~~Su and Gibeaut (2009) classified water points from NIR LiDAR based on point density, intensity and elevation. They identified the shoreline based on the large sudden decrease in NIR LiDAR intensity values when going from land to water. ~~Brzank et al. (2008) used the same three variables (point density, intensity and altitude~~Brzank et al. (2008) used the same three variables (point density, intensity and elevation) in a supervised fuzzy classification to detect the water surface in a section of the Wadden Sea. Another study in the Wadden Sea by (Schmidt et al. (2012)) used a range of geometric characteristics as well as intensity values to classify water points from NIR LiDAR data.

The capability of NIR LiDAR data for detecting the water surface ~~detection~~ is thus well documented. However, deriving all the information ~~(seabed and water surface)~~ from a single green LiDAR dataset would be a more effective solution for water surface and seabed detection, with respect to the financial expenses and for the difficulties of storing and handling often very large amounts of data. However, there is no definitive method for making a DWSM from green topobathymetric LiDAR data. For this purpose, the Austrian LiDAR company RIEGL have developed a software, *RiHYDRO* (RIEGL, 2015), in which it is possible to model the water surface in a two-step approach: 1) Classification of water surface points based on areas with two layers (water surface and seabed) and extending the classification to the entire water body, and 2) Generation of a geometric gridded ~~water surface model~~DWSM for each flight swath based on the classified water surface points. However, RiHYDRO is commercial software, and thus the algorithms, which form the basis of the classification and water surface modelling, are not publicly available. Other software packages, such as *HydroFusion* (Optech, 2013) and *LiDAR Survey Studio* (Leica, 2015), also proclaim to have incorporated methods for the entire data processing workflow, but the algorithms in these software packages are also closed and cannot be accessed by public users.

~~Only few research studies have investigated the potential of water surface detection from green LiDAR data. Guenther et al. (2000)~~Only few research studies have investigated the potential of water surface detection and modelling from green LiDAR data. In a relatively recent publication Guenther et al. (2000) even regarded water surface detection from green LiDAR data as unacceptable and they justified it with two fundamental issues: 1) No water surface returns are detected in the dead zone, and 2) Uncertainty of the water surface ~~altitude~~elevation, because the green water surface returns are actually a mix of returns from the air/water interface and from volume backscatter returns, and they are generally found as a cloud of points below the water surface. (Mandlburger et al. (2013)) addressed the second issue by comparing the water surface points of NIR and green LiDAR data, and they concluded that it is possible to derive the water surface ~~altitude~~elevation from the green LiDAR data with sub-decimetre vertical precision relative to a reference water surface derived by the NIR LiDAR data. However, their work addressed only the determination of the water surface ~~altitude, without going into detail on the actual procedure of modelling the water surface. An approach for modelling the water surface from green LiDAR data was presented by Mandlburger et al. (2015),~~elevation, without going into detail on the actual procedure of generating a DWSM. An approach for modelling the water surface from green LiDAR data was presented by Mandlburger et al. (2015), who did their study in a riverine environment with only few return signals from the water surface. Their method was based on manual estimates of the water level in a series of river cross sections, after which interpolation between the cross sections filled out the gaps with no water surface points to derive a continuous water surface model. ~~The vertical accuracy of the detected water surface was evaluated by statistical comparison against water surface points from a terrestrial laser scanner, resulting in a root mean square error of ±3.3 cm.~~

~~Published literature that deals with water surface modelling/detection procedure in the coastal zone based solely on green laser Lidar data are very few and the procedure for LiDAR data processing to reach this goal is not clearly explained.~~

The aim of this study was to investigate the potential of improving the ~~processing~~ procedure of processing green LiDAR data ~~for~~and generating DEMs in tidal ~~coastal~~ environments~~ characterised by land-water transition zones~~, and of improving the classification of morphological units in such environments. More specifically, the objectives were:

1. To develop a robust, repeatable and user friendly processing procedure of raw green LiDAR data for generating high resolution DEMs in land-water transition zones.
2. To quantify the accuracy and precision of the green LiDAR data based on object detection.
3. To automatically classify morphological units based on ~~morphometric~~geomorphometric analyses of the generated DEM.

The investigations were based on studies undertaken in a section of the Knudedyb tidal inlet system in the Danish Wadden Sea.

2 Study area

The Knudedyb tidal inlet system is located between the barrier islands of Fanø and Mandø in the Danish Wadden Sea (Fig. ~~2A~~1A). The tidal inlet system is a natural environment without larger influence from human activity. The tides in the area are semi-diurnal, with a mean tidal range of 1.6 m, and the tidal prism is in the order of $175 \cdot 10^6$ m^3 (Pedersen and Bartholdy, 2006). The main channel is approximately 1 km wide and with an average water depth of approx. 15 m (Lefebvre et al., 2013).

The study site is an elongated 3.2 km^2 (0.85 × 4 km) section of the Knudedyb tidal inlet system (Fig. ~~2B~~1B). The section is located perpendicular to the main channel and stretches across both topography and bathymetry. The study site extends towards north into an area on Fanø with dispersed cottages (Fig. ~~2C~~1C). The most prominent morphological features within the study site include beach dunes (Fig. ~~2D~~1D), small mounds (Fig. ~~E~~1E), swash bars (Fig. ~~2F~~1F-G) and linear bars (Fig. ~~2H).The quality of the LiDAR data were validated at two sites along Ribe Vesterå River (Fig. 2I-J):~~1H).

- ~~Validation site 1 is a cement block with a size of 2.50×1.25×0.80 m located on land next to the mouth of Ribe Vesterå River (Fig. 2I). The block was used for assessing the accuracy and precision of the LiDAR data.~~
- ~~Validation site 2 is a steel frame with a size of 0.92×0.92×0.30 m located in the river with the surface just below the water surface (Fig. 2J). The frame was used for precision assessment, and for testing the feature detection capability of the LiDAR system. According to the hydrographic survey standards presented by~~

the International Hydrographic Organization (IHO, 2008), cubic features of at least 1 m^2 should be detectable in Special Order areas, which are areas with very shallow water as in the study site.

3 Methods

3.1 Topobathymetric LiDAR

The topobathymetric LiDAR technique is based on continuous measurements of the distance between an airplane and the ground/seabed. The distance (or range) is calculated by half the travel time of a laser beam, going from the airplane to the surface of the earth and back to the airplane. The wavelength of the laser beam is in the green spectrum, usually 532 nm, since this wavelength is found to attenuate the least in the water column, resulting in the largest penetration depth of the laser (Jensen, 2009). In literature, topobathymetric LiDAR data is sometimes referred to as either bathymetric LiDAR or Airborne LiDAR bathymetry. These are different terms with the same meaning, and in this paper, topobathymetric LiDAR is preferred, since it describes the system's ability to simultaneously measure bathymetry as well as topography.

A single laser beam may encounter many targets of varying nature on its way from the airplane and back again, and different processes are influencing the laser beam propagation through air and water. First, the laser beam may be reflected by targets in the air, such as birds or dust particles, and these can show up as LiDAR points in the space between the airplane and the surface. When encountering water, the speed of the laser decreases from 3×10^8 ms^{-1} to e.g. 2.25×10^8 ms^{-1} in 10°C freshwater or e.g. 2.24×10^8 ms^{-1} in 10°C saltwater of 30 PSU (Millard and Seaver, 1990).

The changing speed of the laser beam also affects the direction of the laser beam when penetrating the water surface with an angle different from nadir (Fig. 2) (Guenther, 2007; Jensen, 2009). The laser beam will be refracted according to Snell's Law:

$$\frac{\sin\alpha_{air}}{\sin\alpha_{water}} = \frac{c_{air}}{c_{water}} = \frac{n_{water}}{n_{air}} \qquad (1)$$

where α_{air} is the incidence angle of the laser beam relative to the normal vector of the water surface and α_{water} is the refraction angle in water. n_{water} and n_{air} are the refractive indices of water and air, respectively (Mandlburger et al., 2013).

The penetration depth in water is limited by the attenuation of the laser beam. Water molecules, suspended sediment and dissolved material all act on the laser beam by absorption and scattering, resulting in substantial reduction in power as the signal propagates into the water (Guenther, 2007; Mandlburger et al., 2013; Steinbacher et al., 2012). The laser beam also diverges in the water column, resulting in a wider laser beam footprint (Guenther et al., 2000), and this effect reduces the resolving capability of fine-scale morphology the deeper the laser beam penetrates.

The returned signal is represented as a distribution of energy over time, also called the 'full-waveform' (Alexander, 2010; Chauve et al., 2007; Mallet and Bretar, 2009). The peaks in the full-waveform are detected as individual targets encountered by the propagating laser beam. If the laser hits two targets with a small vertical difference, such as a water surface and seabed in very shallow water, then the two peaks in the full-waveform may merge together, resulting in the detection of only one target (Fig. 2). This results in a detection minimum of successive returns from a single laser pulse, referred to as the 'dead zone' (Mandlburger et al., 2011; Nayegandhi et al., 2009). The dead zone is a clear limitation to the LiDAR measurements, which is an important parameter to consider in very shallow water, such as intertidal environments.

3.13.2 Surveys and instruments

LiDAR data and ortophotos were collected by Airborne Hydro Mapping GmbH (AHM) during two surveys on 19 April 2014 and 30 May 2014.

On 19 April 2014, validation sites 1 and 2 were covered for accuracy and precision assessmentthe quality of the LiDAR data by object detection of thewas validated at two sites along Ribe Vesterå River (Fig. 1I-J):

- Validation site 1 with a 2.50 × 1.25 × 0.80 m cement block andlocated on land next to the frame (for location see mouth of Ribe Vesterå River (Fig. 21I). The block was covered by 7 swaths retaining 227 LiDAR points from the block surface~~.~~, which were used for assessing the accuracy and precision of the LiDAR data.

- Validation site 2 with a 0.92 × 0.92 × 0.30 m steel frame located in the Ribe Vesterå River, its top situated just below the water surface (Fig. 1J). The frame was covered by 4 swaths retaining 46 LiDAR points from the surface of the frame~~. ~~, which were used for precision assessment, and for testing the feature detection capability of the LiDAR system. According to the International Hydrographic Organization survey standards, cubic features of at least 1 m^2 should be detectable in Special Order areas, which are areas with very shallow water as in the study site (IHO, 2008).

Ground control points (GCPs) were measured for the four corners of the block with accuracy better than 2 cm using a Trimble R8 RTK GPS. Measurements were repeated three times and averaged to minimize errors caused by measurement uncertainties. GCPs were also collected for the frame; however, during the LiDAR survey the frame experienced an unforeseen intervention by local fishermen using the frame as fishing platform. Therefore, the frame ~~is~~was only used to assess the deviation between the LiDAR points (the precision), and not to assess the deviation between the LiDAR points and the GCP’s (the accuracy).

On 30 May 2014, the study site was covered by 11 swaths, which were used for generating the DWSM and DEM. ~~Low~~The overflight was carried out during low tide, and the water level was measured to -1 m DVR90~~, measured~~ at Grådyb Barre, approx. 20 km NW of the study site.

The weather conditions were similar during the two surveys, with sunny ~~periods~~conditions, average wind velocities of 7-8 m/s (DMI, 2014)~~ and approx. 0.5 m wave heights coming from NW, measured west of Fanø (DCA, 2014). The wave heights in the less exposed Knudedyb tidal inlet was observed in the LiDAR data to 0.2-0.3 m. Overall, both days constituted good conditions for topobathymetric LiDAR surveys.~~

~~In both surveys, ~~ and significant wave heights, measured west of Fanø at 15 m water, of approx. 0.5 m coming from NW (DCA, 2014). However, the waves in the less exposed Knudedyb tidal inlet were observed in the 30 May LiDAR point cloud to be 0.2-0.3 m, which can be explained by the location of the study site in lee of the western most intertidal flats and the ebb-tidal delta. The wave heights in the rest of the study site (flood channel and intertidal ponds) were in the scale of sub decimetres. There were no waves at validation site 2 during the 19 April LiDAR survey.

LiDAR data were collected with a RIEGL VQ-820-G topobathymetric airborne laser scanner. The scanner is characterized by emitting green laser pulses with 532 nm wavelength and 1 ns pulse width. It has a very high laser pulse repetition rate of up to 520,000 Hz, and a beam divergence of 1 mrad creates a narrow laser beam footprint of 40 cm diameter at a flying altitude of 400 m in both surveys (RIEGL, 2014), which was the actual flying altitude during the surveys. The high repetition rate and narrow footprint makes it well suited to capture fine scale landforms (Doneus et al., 2013; Mandlburger et al., 2011; RIEGL, 2014). An arc shaped scan pattern results in a swath width of approx. 400 m (at 400 m flying altitude), while maintaining an almost constant 20° (±1°) incidence angle of the laser beam when it penetrates the water surface . The scanner was characterized by emitting green laser pulses with 532 nm wavelength and 1 ns pulse width. It had a very high laser pulse repetition rate of up to 520,000 Hz. The flying altitude was 400 m, which combined with a beam divergence of 1 mrad created a laser beam footprint of 40 cm diameter at the ground. The high repetition rate and narrow footprint made it well suited to capture fine-scale landforms (Doneus et al., 2013; Mandlburger et al., 2011). An arc shaped scan pattern results in a swath width of approx. 400 m, while maintaining an almost constant 20° (±1°) incidence angle of the laser beam when penetrating the water surface (Niemeyer and Soergel, 2013). The typical water depth penetration of the laser scanner is 1 Secchi disc depth.

. The typical water depth penetration of the laser scanner is claimed by the manufacturer to be 1 Secchi disc depth (RIEGL, 2014).

For each returned signal, the collected LiDAR data contained information of x, y and z, as well as a GPS time stamp and values of the amplitude, reflectance, return number, attribute and laser beam deviation (RIEGL, 2012).

~~3.2~~3.3 Processing raw topobathymetric LiDAR data into a gridded DEM

The essential processing steps, which are standard procedure when processing topobathymetric LiDAR data, were followed to produce a DEM in the study area. These steps included:

1. Determination of flight trajectory.
2. Boresight calibration: Calculating internal scanner calibration.
3. Collecting topobathymetric LiDAR data.
4. Swath alignment based on boresight calibration: The bias between individual swaths was minimized.
5. Filtering: The raw data contained noise located both above and below ground, which needed to be filtered from the point cloud.
6. Water surface detection: A ~~water surface~~DWSM had to be established in order to correct for refraction in the following step.
7. Refraction correction: All the points below the water surface in the DWSM were corrected for the refraction of the laser beam.
8. Point cloud to DEM: The points were transformed into a ~~surface~~gridded elevation model representing the real world ~~topography~~terrain in the study area, including cottages and ~~bathymetry~~vegetation on Fanø in the northern part.

Step 1 and 2 were performed prior to the LiDAR survey. The different instruments (LiDAR, IMU and GPS) were integrated spatially by measuring their position relative to each other, when mounted on the airplane, and temporally by calibrating their time stamps.

Step 3 was the actual LiDAR survey and step 4 was the initial processing step after the LiDAR survey. The bias between the swaths was minimized in the software RiPROCESS (RIEGL LMS) by automatically searching for planes in each swath and then matching the planes between the swaths.

~~Step~~Steps 5-8 ~~represents~~represent the processing of the point cloud into a DEM. The methods involved in these steps are the main focus in this ~~work~~study and they are described in detail in the following sub-sections. Each swath was pulled individually through the processing workflow to account for the continually changing water level in the study area due to tides. The broad term "DEM" is used, rather than the more specific terms “Digital Terrain Model (DTM)” or “Digital Surface Model (DSM)”, because the generated model includes both natural terrain in the tidal environment, which is the main focus area in this study, as well as vegetation and cottages on Fanø.

3.2.13.3.1 Filtering

The raw LiDAR data contained noise in the air column originating from the laser being scattered by birds, clouds, dust and other particles, and noise was also appearing below the ground/seabed (Fig. 3A-B). This noise had to be filtered before further processing. The filtering process involved both automatic and manual filtering.

1. Automatic filtering

The automatic filtering was carried out in HydroVish (AHM) with the tool *Remove flaw echoes* (Fig. 3C). The filtering tool was controlled by three variable parameters: search radius, distance and density. The search radius parameter specified the radius of a sphere in which the distance and density filters were utilized. The distance parameter rejected a point, if it was too far from any other point within the sphere. The density parameter specified the lower limit of points within the sphere. The automatic filter iterated through all the points in the point cloud.

~~In order to identify the best settings of the three parameters, a sensitivity analysis was performed on three data fragments representing different natural environments in the Knudedyb tidal inlet system: a fragment in the flood channel, one on the tidal flat and a fragment with vegetation. The outcome of the filtering was compared for different settings to decide the most suitable settings to use for filtering the whole study area. It was not possible to reach a specific setting, which would be optimal for all the different environments. Particularly, the deeper bathymetric parts contained more widely dispersed points, which were easily rejected by the filter. The analyses with different settings also showed that two layers of noise close to the ground, both above and below, were very difficult, if not impossible, to reject with this automatic filtering method. The settings were selected so that a minimum of valid points were rejected~~ The settings for the automatic filtering were based on a sensitivity analysis of three fragments of the LiDAR data, and the settings were selected so that a minimum of valid points were removed by the automatic filter. The settings were: Search radius = 1 m, distance = 0.75 m and density = 4.

~~2. Manual filtering~~

~~The remaining noise was manually filtered in the software Fledermaus (QPS) (Fig.~~The automatic filter could not to remove two layers of noise points close above and below ground, but on the other hand, more widely dispersed points in the deeper bathymetry were removed. To account for this, the point cloud went through manual filtering in Fledermaus (QPS) software, where the remaining noise points were rejected and the valid bathymetric points were accepted (Fig. 3D).

The filtered point cloud (with water points) was used in the following step to detect the water surface. Meanwhile, a copy of the data ~~were~~was undergoing additional manual filtering, removing all the water points (Fig. 3E). After this final filtering step, there were only points representing topography, bathymetry, vegetation and man-made structures left in the dataset.

~~3.2.2~~3.3.2 Water surface detection

The water surface detection was based on determining the water surface ~~*altitude*~~*elevation* and the water surface *extent*~~.~~, thereby producing a DWSM. The water surface ~~altitude~~elevation was determined based on the water surface points, and the extent was determined by extrapolating the water surface until it intersected the surface of the topography. Two assumptions ~~about the water surface~~ were made in the production of the DWSM:

1. The water surface was horizontal. This was a simplification of the real world. Tidal processes and wind- and wave-setup may cause the water surface to be sloping, and the water is often topped by more or less significant ~~wave action~~waves. A linear fit through the water surface LiDAR points along the main channel, showed a changing water level of 0.13 m over a distance of 400 m, corresponding to a 0.325×10^{-3} (0.019 deg.) sloping water surface. A similar fit through the LiDAR points along the flood channel showed a slope of 0.156×10^{-3} (0.009 deg.). The maximum wave heights observed in the main channel were 20-30 cm. Based on the moderate slope of the water surface and relatively low wave height, the water surface was assumed flat. This assumption is deemed error prone, but at the time of this study, it was ~~currently~~ our best estimate.
2. The study area contained water bodies with two different water levels: One represented the water level in the main channel and the other represented the water level in the flood channel. This was also a simplification, as the tidal flat contained small ponds with potentially different water levels. However, almost all of these ponds contained no LiDAR points of the water surface, which means that the water depth in the ponds must have been within the limitation of the dead zone. Therefore, it was impossible to detect individual water surfaces in the ponds.

A series of processing steps were performed to ~~detect~~produce the ~~water surface~~DWSM. The first step was to extract a *shallow surface* and a *deep surface* from the filtered point cloud (with water points) in Fledermaus (Fig. 3F). Both surfaces consisted of 0.5 × 0.5 m cells, and the ~~altitude~~elevation of each cell was equal to the highest point within the cell (shallow surface) and the lowest point within the cell (deep surface), respectively. The shallow surface should then display the topography along with the water surface, whereas the deep surface should display the topography and the seabed (as long as the seabed was detected by the laser). It is worth noting, that the extraction of the shallow surface and the deep surface ~~have~~had nothing to do with the final DEM, as they ~~are just~~were merely intermediate steps performed for the water surface detection.

The following steps were focused on the shallow surface to determine the ~~altitude~~elevation of the water surface (Fig. 3G). First, the shallow surface was down-sampled to a surface with a cell size of 2 × 2 m, and the new cells were populated with the maximum ~~altitude~~elevation of the input cells. The down-sampling was done for smoothing the water surface, and thereby eliminating most of the outliers. The exact cell size of 2 × 2 m, as well as populating them with the maximum value, was chosen based on the work by ~~Mandlburger et al. (2013).~~Mandlburger et al. (2013). They compared water surface detection capability between green LiDAR data, collected with the same RIEGL-VQ-820-G laser scanner, and NIR LiDAR data, which was assumed to capture the true water surface. They found that the green LiDAR generally underestimated the water surface ~~level~~elevation, but that reliable results were achieved by increasing the cell size and only taking the top ~~95-100~~1-5% of water points into account. According to their work, it was assumed that placing the water surface on the highest points in 2 m cells provided a good estimate of the true water level. However, based on their results it could be expected that the water surface ~~level~~elevation in this case would be underestimated in the order of 2-4 cm.

The water~~-~~-covered areas in the main channel and the flood channel were manually extracted from the newly down-sampled ~~raster~~shallow surface. The average ~~altitude~~elevation of the 2 m cells within each area was calculated~~ individually in each area~~, and these values constituted the elevation of the water ~~surface levels~~surfaces in the main channel and in the flood channel, respectively.

~~Hereafter, the extent of the water surfaces was determined (Fig. 3H).~~ Two horizontal water surfaces were created in the flood channel and the main channel with a cell size of 0.5 × 0.5 m and cell values equal to the ~~determined~~calculated water surface ~~altitudes in each region.~~elevations. The high spatial resolution of 0.5 m cells was chosen to produce a detailed ~~water surface~~DWSM along the edges of the land-water transition~~. It also made the calculations in the following step straightforward, because the resolution was similar to that of the deep surface. The deep surface cell altitudes were subtracted from the water surface altitude and all cells with resulting negative values were discarded from the water surface. Thereby, all the water surface cells which were below the deep surface were discarded. All the cells above the deep surface were expected to represent the two water surfaces. Thereby, two water surfaces were created; one in the main channel and one in the flood channel~~.

Finally, the extent of the water surfaces was determined by subtracting the deep surface cell elevations from the water surface elevation and discarding all cells with resulting negative values (Fig. 3H), together forming the DWSM.

~~3.2.3~~3.3.3 Refraction correction

The refraction correction of all the points below the ~~water surfaces~~DWSM was calculated in HydroVish (AHM). The input parameters were the filtered point cloud (without water points), the derived ~~water surfaces~~DWSM and the trajectory data of the airplane.~~ These were all converted to F5 file format to allow import into HydroVish (AHM).~~ The refraction correction was calculated automatically for each point based on the water depth, the incident angle of the laser beam, and the refracted angle according to Snell's Law (Eq. 1 and Fig. 3I).

~~3.2.4~~3.3.4 Point cloud to DEM

After iterating through the processes of filtering, water surface detection and refraction correction for all the individual swaths, the LiDAR points of all swaths were combined. The transformation from point cloud into a DEM was performed with ArcGIS (ESRI) software. The DEM was created as a raster surface with a cell size of 0.5 × 0.5 m, and each cell was attributed the average ~~altitude~~elevation of the points within the cell-boundaries. It was chosen to make the resolution of the DEM lower than the laser beam footprint size (i.e. 40 cm), due to the inaccuracies arising from attributing smaller cells with measured ~~altitude~~elevation values spanning across a larger area. Furthermore, the 0.5 m cell size was chosen to get as high resolution as possible without making any significant interpolation between the measurements. In this way, each cell represented actually measured ~~altitudes~~elevations instead of interpolated values. However, there were still very few gaps of individual cells with no data in the resulting raster surface in areas with relatively low point density. Despite of the general intention of avoiding interpolation it was chosen to populate these cells with interpolated values to ~~end up with~~obtain a full ~~DEM~~ coverage DEM (except for the bathymetric parts beyond the maximum laser penetration depth). The arguments for interpolation were that: 1) the interpolated cells were scattered and represented only 1.7 % of all the cells, 2) they were found primarily on the tidal flat where the slope is generally less than 1°, meaning that the ~~altitude~~elevation difference from one cell to a neighbouring cell is usually less than 1 cm, and 3) the general point density in most of the study area was so high that the loss of information by lowering the DEM resolution would represent a larger sacrifice than interpolating a few scattered cells. The interpolation was performed by assigning the average value of all neighbouring cells to the empty cells. The final DEM was thereby fully covering the topography, and the bathymetry was covered down to a depth equal to the maximum laser penetration depth.

~~3.3~~3.4 Accuracy and precision of the topobathymetric LiDAR data

The term *accuracy* refers to the difference between a point coordinate (in this case a LiDAR point) compared to its "true" coordinate measured with higher accuracy, e.g. by a total station or a differential GPS; while the term *precision* refers to the difference between successive point coordinates compared to their mean value, i.e. the repeatability of the measurements (Graham, 2012; Jensen, 2009; RIEGL, 2014).

Two "best-fit planes" based on the LiDAR points on the block and the frame surfaces were established with the *Curve Fitting tool* in MATLAB (MathWorks). We propose the use of these two planes to give an indication of the relative precision of the LiDAR measurements.

Another best-fit plane was established based on the block GPS measurements, and this plane was regarded as the "true" block surface for assessment of the accuracy of the

LiDAR measurements. The established planes were described by the polynomial equation:

$$z(x, y) = \mathrm{a} + \mathrm{b}x + \mathrm{c}y \tag{2}$$

where x, y and z are coordinates and a, b and c are constants. Inserting x and y coordinates for the LiDAR surface points in Eq. (3) led to a result of the corresponding ~~altitude~~elevation (z) as projected on the fitted plane. The difference between the ~~altitude~~elevation of the LiDAR point and the corresponding ~~altitude~~elevation on the fitted plane was used as a measure of the vertical accuracy (for the GCP fitted plane of the block) and the vertical precision (for the LiDAR point fitted plane of the block and the frame). Statistical measures of the standard deviation (σ), mean absolute error (E_{MA}), and root mean square error (E_{RMS}) were calculated by:

$$\sigma = \sqrt{\frac{\sum (z_{\mathrm{i}} - z_{\mathrm{plane}})^2}{n-1}} \tag{3}$$

$$E_{\mathrm{MA}} = \frac{\sum |z_{\mathrm{i}} - z_{\mathrm{plane}}|}{n} \tag{4}$$

$$E_{\mathrm{RMS}} = \sqrt{\frac{\sum (z_{\mathrm{i}} - z_{\mathrm{plane}})^2}{n}} \tag{5}$$

where z_i is the ~~altitude~~elevation of the measured LiDAR points, z_{plane} is the corresponding ~~altitude~~elevation on the best-fit plane, and n is the number of LiDAR points. The vertical accuracy and precision were determined at a 95% confidence level based on the accuracy standard presented in *Geospatial Position Accuracy Standards Part 3: National Standard for Spatial Data Accuracy* (NSSDA) (FGDC, 1998):

$$CI_{95\%} = E_{\mathrm{RMS}} \cdot 1.96 \tag{6}$$

The horizontal accuracy was determined as the horizontal mean absolute error ($E_{\mathrm{MA,xy}}$) based on the horizontal distances between the block corners, measured with RTK GPS, and the best approximation of the block corners derived from the LiDAR points of the block surface. The minimum distance between a block corner and the perimeter of the LiDAR points was regarded as the best approximation. Hereafter $E_{\mathrm{MA,xy}}$ was calculated as the average of the four corners.

~~3.4~~3.5 Geomorphometric and morphological classifications

The processed DEM was applied in two classification analyses; first a *geomorphometric* classification and then a *morphological* classification. Both were based on the DEM and derivatives of the DEM, but they differentiated by the resulting classification classes, which showed 1) Surface geometry and 2) Surface morphology. ~~-~~ The analysis mode, as defined by Pike et al. (2009), was "general" in the geomorphometric classification where the surface geometry was continuously classified within the study site, while being "specific" in the morphological classification where discrete morphological units were classified. The northern part of the study site with cottages on Fanø was excluded in the classification analyses, as the objective of this work was to classify the natural terrain (geomorphometry and morphology) in the high-energy and dynamic tidal environment.

3.5.1 Geomorphometric classification analysis

The tool Benthic Terrain Modeler (BTM) (Wright et al., 2005) was used for the geomorphometric classification. The tool is an extension to ArcGIS Spatial Analyst, originally used for analysing MBES data (Diesing et al., 2009; Lundblad et al., 2006; Rinehart et al., 2004). The BTM classification tool uses fine- and broad~~-~~-scale Bathymetric Positioning Indexes (BPIs) (Verfaillie et al., 2007) in a multiple~~-~~-scale terrain analysis to classify fine- and broad~~-~~-scale geometrical features. The BPIs are measures of the ~~altitude~~elevation of a cell compared to the ~~altitude~~elevation of the surrounding cells within the determined scale (radius) size. Positive BPI values indicate a higher ~~altitude~~elevation than the neighbouring cells and negative BPI values indicate a lower ~~altitude~~elevation than the neighbouring cells. For instance, a BPI value of 100 corresponds to 1 standard deviation and a value of -100 corresponds to -1 standard deviation of the cell elevation compared to the elevation of the surrounding cells within the determined scale size. BPI values close to zero are derived from flat areas or from constant slopes.

The ~~altitude~~elevation values of each cell in the DEM ~~was~~were exaggerated by a factor of 10 ~~times~~ before the classification, to enable the BTM to detect the shapes of the ~~landscape~~terrain. The fine- and broad~~-~~-scales were determined based on the BPI results for different radius sizes. The best results were obtained from a broad~~-~~-scale BPI of 100 m radius and a fine~~-~~-scale BPI of 10 m radius~~.~~, based on visual inspection. The fine- and broad~~–~~-scale BPIs were used, together with the slope of the actual DEM ~~derived slopes~~(not the exaggerated) to classify the investigated area into the geomorphometric classes: ~~Small~~Fine-scale crests, ~~large~~broad-scale crests, depressions, slopes and flats (Fig. 4). The classification classes were decided based on previous studies using the BTM classification tool with success (Diesing et al., 2009; Lundblad et al., 2006). The thresholds for the fine- and broad~~-~~-scale BPIs were in previous studies often defined as 1 standard deviation (Lundblad et al., 2006; Verfaillie et al., 2007), however, thresholds of 0.5 standard deviations have also previously been applied (Kaskela et al., 2012). We used a low threshold of 0.5 standard deviations due to the generally very gentle variations in the ~~landscape~~terrain geometry of the tidal inlet system. We defined the threshold between slopes and flats as 2°. This definition was a compromise between detecting as many slopes as possible but avoiding too many “false slopes” being detected along the swath edges, which seemed to be a consequence of lower precision at the outer beams of the swath, as well as differences between overlapping swaths.

3.5.2 Morphological classification analysis

A morphological classification was developed for ~~the purpose of~~ delineating ~~classes of~~ actual morphological features in the study area. ~~This~~The classification was built partly on different neighbourhood analyses and slopes derived from the DEM, and partly on the local tidal range. ~~Large-~~Broad-scale crests from the geomorphometric classification were also incorporated in the analysis. Figure 5 describes the steps performed in ArcGIS, which led to the classification of 6 morphological classes: Swash bars, linear bars, beach dunes, intertidal flats, intertidal creeks and subtidal channels. All the criteria for defining a particular morphological class had to be fulfilled for a cell to be classified into that class. Cells that did not meet the criteria to be classified into any of the morphological classes were assigned the class “unclassified”.

33 years of continuous measurements of the water level at Havneby on Rømø, 25 km south of the study area, ~~shows~~showed a mean low water level of -0.94 m (DVR90) and a mean high water of 0.94 m (DVR90) (Klagenberg et al., 2008). Although the tidal range in Knudedyb ~~is~~was probably slightly different, it ~~is~~was the best estimate for the

study site. Therefore, these water levels were used to separate between the supratidal, intertidal and subtidal zones.

Subtidal channels were defined as everything below the mean low water, which ~~is~~was -0.94 m. A "smooth DEM" was created, in which each cell of the original DEM was assigned the average ~~altitude~~elevation value of its surrounding cells in a window size of ~~100x100~~100 × 100 m~~.~~ (actually 199 × 199 cells, i.e. 99.5 × 99.5 m). The result was subtracted from the original DEM, creating an Elevation Change Model (ECM), which made it possible to extract information about the deviation of the cells in the DEM compared to its surrounding cells. The principle is similar to the BPI, and again the purpose was to locate cells, with a higher/lower ~~altitude~~elevation than its surrounding cells. Positive values were higher cells and negative values were lower cells. Certain thresholds were found suitable for classifying beach dunes (> 0.8 m) and intertidal creeks (< -0.3 m). These two classes were furthermore classified into their respective tidal zones (supratidal and intertidal) based on the ~~altitude~~elevation. Intertidal flats were classified by low slope values (< 1°) of a down-sampled 2 m DEM (each down-sampled cell was assigned the mean value of its ~~4x4~~4 × 4 original cells). Moreover, to be classified as a flat, the ECM ~~has~~had to be within ±10 cm to avoid any incorrect intertidal flat classification of flat crests on top of bars or flat bottoms inside creeks or channels. The BTM classification class "~~large~~broad-scale crests" ~~is~~was used as an input, since it ~~is~~was found to capture bar features. However, the thresholds used in the BTM classification resulted in capturing features larger than bars in the ~~large~~broad-scale crests class. To distinguish between bars and larger features, the standard deviation of each DEM cell in a moving window size of ~~250x250~~250 × 250 m ~~is~~(actually 249 × 249 cells, i.e. 124.5 × 124.5 m) was calculated. A suitable threshold to distinguish between bars and larger features ~~are~~was 0.6 standard deviations. Finally, swash bars and linear bars ~~are distinguished~~were identified by an area/perimeter-ratio, based on the assumption that linear bars ~~has a~~have smaller ratio than swash bars, due to the different shapes. ~~In this case,~~Based on visual interpretation, a ratio of 4 ~~were~~was found to be a suitable ~~ratio~~ threshold.

4 Results

4.1 Refraction correction and dead zone extent

The vertical adjustment of the LiDAR points (z_{diff}) due to refraction correction ~~(z_{diff})~~ is linearly correlated with the water depth (d) (Fig. 6). An empirical formula ~~was~~is derived for this relationship~~ and is given by the equation~~:

$$z_{\mathrm{diff}} = 0.227 \cdot d\ ,\ \mathrm{R}^2 = 0.997 \qquad (7)$$

A LiDAR point at 1 m water depth is vertically adjusted by approximately 0.23 m (Fig. 6). The variations around the linear trend in Fig. 6 are due to changing incidence angles of the laser beam that varies with the airplane attitude (roll, pitch and yaw).

The vertical extent of the dead zone is approx. 28 cm, determined by plotting the vertical difference between the shallowest and the deepest LiDAR point within 0.5 m cells – i.e. between the shallow surface and the deep surface (Fig. 7). The difference is manifested by an abrupt change at the dead zone, and the highest rate of change is shown to be at a water depth of approx. 28 cm.

4.2 Sub-decimetre accuracy and precision

The vertical root mean square error of the LiDAR data is ±4.1 cm, and the accuracy is ±8.1 cm with a 95% confidence level (Table 1 and Fig. 8A). The vertical precision of the LiDAR data with a 95 % confidence level is ±3.8 cm for the points on the frame, and ±7.6 cm for the points on the block (Table 1).

The horizontal accuracy calculated as the horizontal mean absolute error ($E_{\mathrm{MA,xy}}$) is determined to ±10.4 cm~~, which is the average of the minimum distances between the four block corners and the edge of the block surface derived by the LiDAR data (Fig.~~ (Fig. 8B).

4.3 Point density and resolution

The average point density is 20 points per m^2, which equals an average point spacing of 20 cm (Table 2). The point density of the individual swaths varies between 7-13 points per m^2, and the point density of the combined swaths in the study area, varies between 0-216 points per m^2, although above 50 points per m^2 are rare.

4.4 DEM and landforms

The ~~altitudes~~elevations in the studied section of the Knudedyb tidal inlet system range from -4 m DVR90 in the deepest parts of the flood channel and main channel to 21 m DVR90 on top of the beach dunes on Fanø (Fig. 9). Beach dunes and cottages of the village Sønderho are clearly visible in the northern part of the study site (Fig. 9A-B). The intertidal ~~areas~~zones are generally flat, while the most varying morphology is found in the area of the flood channel (Fig. 9C-D), and in the area close to the main channel (Fig. 9E-F). The flood channel is approximately 200 m wide in the western part and it divides into two channels towards east. The bathymetry of the channel bed is clearly captured by the LiDAR data in the eastern part, and also in the western part down to -4 m DVR90, which approximately equals a water depth of 3 m at the time of survey. An intertidal creek joins the flood channel from the north (Fig. 9D). From the flood channel towards south, the tidal flat is vaguely upward sloping, until reaching two distinct swash bars, which are rising 0.9 m above the surrounding tidal flat, reaching a maximum ~~altitude~~elevation of 1.5 m DVR90 (Fig. 9E-F). Further south, the linear bars along the margin of the main channel are clearly captured in the DEM (Fig. 9E).

4.5 Geomorphometric and morphological classifications

The geomorphometric and morphological classifications show that most of the study ~~site~~area is located in the intertidal zone, and is mostly flat. ~~That~~This is manifested by the dominating two classes; flats and intertidal flats (Fig. 10A-B). The geomorphometric classification identifies slopes as stripes with NNW-SSE directionality across the flats. These are following the direction of the survey lines, and thus, they are not real morphological features but more an indication of lower precision of the LiDAR data, especially at the outer beams of the swath. These swath artefacts are smoothed out in the morphological classification by down-sampling the DEM to 2 m resolution, and therefore, the intertidal flats appear uniform and seamless. The bar features close to the main channel are well defined in the geomorphometric classification where they are classified as ~~large~~broad-scale crests and ~~small~~fine-scale crests surrounded by slopes. In the morphological classification, these are identified based on neighbourhood analyses and separated by the area/perimeter-ratio into two classes, swash bars and linear bars (Fig. 10C). ~~Large~~Broad-scale crests are also found on Fanø in the northern part of the area, and most of these are classified as beach dunes in the morphological classification. The geomorphometric classification identifies more ~~large~~broad-scale crests along the banks of the flood channel, however, these are not ~~actual~~real bar features but they are identified as crests due to the nearby flood channel and creeks resulting in a positive broad~~-~~-scale BPI. In the morphological classification it is possible to distinguish between these ~~“false” crests~~ and the actual bar features, by looking at ~~altitude~~elevation deviations at an even ~~larger~~broader scale than the broad~~-~~-scale BPI. The intertidal creek in the NWern part of the area is a mix of depressions, slopes and ~~small~~fine-scale crests in the geomorphometric classification, whereas it is relatively well defined and properly delineated in the morphological classification (Fig. 10D).

The geomorphometric classification identifies slopes along the banks of the main channel, flood channel and the intertidal creek, as well as in front of the beach dunes and along the edges of the swash bars and linear bars. The slopes seem particularly reliable at delineating the features in the intertidal zone~~;~~, i.e. swash bars, linear bars and creeks. Depressions are primarily identified in the deepest detected parts of the main channel and in the flood channel, in the intertidal creek and in the beach dunes. ~~Small~~Fine-scale crests are found in the geomorphometric classification in locations which are high compared to its near surroundings. They are primarily seen as parts of the linear bars close to the main channel, in the beach dunes on Fanø and along the banks of the intertidal creeks.

A few small circular ~~patches~~mounds of approx. 5 m diameter with patches of *Spartina Townsendii* (Common Cord Grass) located on the intertidal flat are classified as ~~small~~fine-scale crests in the geomorphometric classification (Fig. 11). It clearly shows the capability of capturing ~~relatively small~~fine-scale features in the DEM and in the derived classification.

5 Discussion

5.1 Performance of the water surface detection method

The water surface in topobathymetric LiDAR surveys is most often detected from NIR LiDAR data, which is simultaneously collected along with the green LiDAR data (Collin et al., 2012; Guenther et al., 2000; Parker and Sinclair, 2012; Wang and Philpot, 2007). However, detecting the water surface and generating a DWSM based on the green LiDAR data alone provides a potential to perform topobathymetric surveys with just one sensor, thus optimizing the survey costs as well as data handling and storage.

The two critical issues risen by ~~Guenther et al. (2000),~~Guenther et al. (2000), as mentioned in the introduction, concerning the water surface detection with green LiDAR were thoroughly investigated in this study. The first issue, regarding the gap of detected water surface signals in the dead zone, is addressed by detecting the water surface based on areas which are known to be covered by water, and thereafter extending the water surface until it intersects the topography, so that also the dead zone is covered by the modelled water surface. The second issue, regarding uncertainty in the water surface ~~altitude determination, is addressed using the results presented byMandlburger et al. (2013)~~elevation determination, is addressed using the results presented by Mandlburger et al. (2013) who found a statistical relationship between the cloud of water surface points in the green LiDAR data and the water surface ~~altitude derived from NIR LiDAR data. Mandlburger et al. (2013)~~elevation derived from NIR LiDAR data. Mandlburger et al. (2013), however, did not describe the actual method of modelling ~~the water surface, which is done in this study. Mandlburger et al. (2015)~~a DWSM, which is done in this study. Mandlburger et al. (2015), on the other hand, did propose a method for modelling the water surface, however, it was done in a fluvial environment and the water level was based on manual determinations of cross sectional water levels. The water surface detection method in this study is thus new in combining the properties: 1) It is only using green LiDAR data, 2) it is based on automatic water level determination, 3) it is applied in a tidal environment (can be applied in any coastal environment) and 4) it is ~~open~~transparent and repeatable due to the ~~public and described~~detailed description of data processing steps given in ~~detail~~the text.

The developed water surface detection method is new but it must be pointed out that the assumption of a flat ~~water surface~~DWSM leaves room for improvements for the future, especially if it is applied in a fluvial environment. Assuming a flat water surface is indeed a simplification of the real world, since the water surface in reality can be inclined, and it can be topped by waves.

5.2 Implications of the dead zone

The vertical extent of the dead zone is in this study determined to approx. 28 cm (Fig. 7), which means that no return signal is detected from the water surface when the water depth is less than 28 cm. ~~As Guenther et al. (2000) explains, the dead zone poses a real challenge to the modelling of a water surface, because all submerged points, also those in less than 28 cm water depth, have to be corrected for refraction. With the water surface detection method proposed in this work this issue has been dealt with by extending the water surface into the dead zone, which makes it possible to correct the LiDAR points in 0-28 cm water depth for refraction. In this way, the implication of the dead zone along the channel edges is diminished, which is particularly beneficial in flat areas such as the Knudedyb tidal inlet system, where the dead zone may cover large areas depending on the tide (Fig. 12).~~

The implication of the dead zone along the channel edges is minimised by extending the DWSM until it intersects the topography, but the setting is different for the small ponds on the intertidal flats. They may have different water levels than in the large channels, but no detected water surface points, since the water depth in the ponds are generally less than the vertical extent of the dead zone, i.e. approx. 28 cm. The presented method is not capable of detecting a water surface in these ponds, which means that the bottom points of the ponds are not corrected for refraction. ~~According to the calculated refraction (Fig. 6), omitting~~Omitting refraction correction of a 28 cm deep pond will result in -6 cm ~~altitude~~elevation error ~~(naturally less error in shallower water).~~ according to the calculated refraction (Fig. 6).

5.3 Evaluation of the topobathymetric LiDAR data quality

The vertical accuracy of conventional topographic LiDAR data has previously been determined to ±10-15 cm ~~(Hladik and Alber, 2012; Jensen, 2009; Klemas, 2013; Mallet~~

~~and Bretar, 2009)~~(Hladik and Alber, 2012; Jensen, 2009; Klemas, 2013; Mallet and Bretar, 2009). Only few previous studies have focused on the accuracy of shallow water topobathymetric LiDAR data ~~(Mandlburger et al., 2015; Nayegandhi et al., 2009; Steinbacher et al., 2012)~~(Mandlburger et al., 2015; Nayegandhi et al., 2009; Steinbacher et al., 2012)~~. Nayegandhi et al. (2009)~~. Nayegandhi et al. (2009) determined the vertical E_{RMS} of LiDAR data in 0-2.5 m water depth to ±10-14 cm, which is above the ±4.1 cm E_{RMS} found in this study (Table 1). ~~Steinbacher et al. (2012)~~Steinbacher et al. (2012) compared topobathymetric LiDAR data from a RIEGL VQ-820-G laser scanner with 70 ground-surveyed river cross sections, serving as reference, and found that the system's error range was ±5-10 cm, which is comparable to the ±8.1 cm accuracy found in this study. ~~Mandlburger et al. (2015)~~Mandlburger et al. (2015) compared ground-surveyed points from a river bed with the median of the four nearest 3D-neighbors in the LiDAR point cloud, and they found a standard deviation of 4.0 cm, which is almost equal to the ±4.1 cm standard deviation found in this study (Table 1). In comparison with these previous findings of LiDAR accuracy, the assessment of the vertical accuracy in this study indicates a good quality of the LiDAR data.

Mapping the full coverage of tidal environments, such as the Wadden Sea, ~~require~~requires a combination of topobathymetric LiDAR to capture topography and shallow bathymetry and MBES to capture the deeper bathymetry. The two technologies make it possible to produce seamless coverage of entire tidal basins; however, merging the two products raises the question whether the quality of the data from the two different sources is comparable. Comparing the LiDAR accuracy with previous findings of accuracy derived from MBES systems indicates similar or slightly better accuracy from the MBES systems ~~(Dix et al., 2012; Ernstsen et al., 2006a)~~(Dix et al., 2012; Ernstsen et al., 2006)~~. Dix et al. (2012)~~. Dix et al. (2012) determined the vertical accuracy of MBES data by testing the system on different objects and in different environments, and found the vertical E_{RMS} to be ±4 cm. Furthermore, they tested a LiDAR system on the same objects and found a similar vertical E_{RMS} of ±4 cm. The vertical E_{RMS} of ±4.1 cm found in this study is very close to both the MBES accuracy and LiDAR accuracy determined by ~~Dix et al. (2012)~~Dix et al. (2012). Another study by ~~Ernstsen et al. (2006a)~~Ernstsen et al. (2006) determined the vertical precision of a high-resolution shallow-water MBES system based on 7 measurements of a ship wreck from a single survey carried out in similar settings as the present study, namely in the main tidal channel in the tidal inlet just north of the inlet investigated in this study. They found the vertical precision to be ±2 cm, which is slightly better than the vertical precision of ±3.8 cm (frame) and ±7.6 cm (block) found in this study. Overall, accuracy and precision are within the scale of sub decimetres for both topobathymetric LiDAR and MBES systems, which enables the mapping of tidal basins with full coverage and with comparable quality.

Due to technical and logistical reasons, the data validation and the actual survey were carried out on different days and in different locations. Based on this, it is a fair question to ask, whether the determined quality actually represents the quality of the data within the study site. ~~In order to address this issue, the environmental conditions~~ Differences between the ~~two surveying dates, as well as the environmental differences, which may impact the~~determined data quality~~, between the study site and~~ at the validation sites ~~are~~ and the data quality at the study site may arise from 1) different environmental conditions on the two surveying days and/or 2) different environments at the validation sites compared~~.~~ to the study site.

~~The environmental conditions in the two surveying days were similar, with sunny conditions, average wind velocities of 7-8 m/s (DMI, 2014) and significant wave heights, measured west of Fanø at 15 m water, of approx. 0.5 m coming from NW (DCA, 2014). However, the waves in the main channel, next to the study site, have been observed in the 30 May LiDAR point cloud to be not more than 0.2-0.3 m, which can be explained by the location of the study site in lee of the western most intertidal flats and the ebb-tidal delta. The wave heights in the rest of the study area (flood channel and intertidal ponds) were in the scale of sub decimetres. In comparison, there were no waves at validation site 2 in Ribe Vesterå River during the 19 April LiDAR survey. As already mentioned, the proposed water surface detection method has a shortcoming of not modelling the waves, and this is a source of error in areas exposed to waves. The precision of the seabed points within the study area are therefore expected to be worse than the ±3.8 cm precision determined at validation site 2, because of the larger wave exposure.~~

The environmental conditions were similar on the two surveying days (as mentioned in the section “Surveys and instruments”), meaning that the different days are not affecting the representation of the data quality within the study site.

The environmental differences between validation site 2 and the study site include the presence of up to 0.2-0.3 m waves in the main channel next to the study site. The waves introduce a source of error, because the proposed water surface detection method is not modelling the waves. The precision of the seabed points within the study site are therefore expected to be worse than the ±3.8 cm precision determined at validation site 2.

The water clarity/turbidity impacts the accuracy of the LiDAR data negatively, due to scattering on particles in the water column, which causes the laser beam to spread ~~(Kunz et al., 1992; Niemeyer and Soergel, 2013)~~(Kunz et al., 1992; Niemeyer and Soergel, 2013). Moreover, part of the light is reflected in the direction of the receiver, and such return signals can be difficult to distinguish from the seabed return ~~(Kunz et al., 1992)~~(Kunz et al., 1992). The turbidity was measured at validation site 2 and in the flood channel close to the study site during the 19 April survey by collecting water samples and subsequently analysing the samples for suspended sediment concentration (SSC) and organic matter content (OMC). The analyses showed that the average SSC was higher in the flood channel (17.2 mg/kg) than in the river (10.2 mg/kg). In contrast, the average OMC was lower in the flood channel (25.5 %) than in the river (40.0 %). These observations indicate that 1) the underwater precision is assessed in a location with higher turbidity than the environment within the study site; therefore, the turbidity cannot be a cause of lower precision in the study site, and 2) the penetration depth seems to be controlled by the OMC rather than by the SSC. This is new knowledge, since no previous studies (from what we know) have investigated the relative effect of organic matter as opposed to inorganic matter on the laser beam penetration depth. However, in order to determine the relationship with statistical confidence, a more comprehensive study is needed, involving measurements of penetration depth at different SSCs and OMCs, and without disturbance from other environmental parameters.

5.4 Spatial variations of topobathymetric LiDAR data quality

The quality of spatial datasets is often provided as single values, such as ±8.1 cm for the vertical accuracy in this case, and then the determined value represents the accuracy/precision of the whole dataset. However, in reality the value is only a measure of the local quality at the location where the assessment is conducted. The quality of the dataset varies spatially, and one way to illustrate ~~that~~this is to extract the maximum vertical difference between the LiDAR points of the processed point cloud within every 0.5×0.5 m cell throughout the study site (Fig. ~~13~~12). In flat areas, without multiple return signals, this shows the spatially varying precision of the dataset. There are large differences on Fanø, which is expected due to vegetation causing multiple LiDAR returns from both the vegetation canopy and from the bare ground. In contrast, the differences on the very gently sloping, non-vegetated tidal flat are up to 10 cm, and there is no simple and natural reason for ~~that~~this variation. A range of factors contribute to the observed variations:

Laser beam incidence angle: The incidence angle, at which the laser beam hits the ground/seabed, is determined by a combination of the scan angle, the water surface angle and the terrain slope. The shape of the footprint is stretched with larger incidence angles, and this effect can cause pulse timing errors in the detected signal, which leads to a decreasing vertical accuracy ~~(Baltsavias, 1999)~~(Baltsavias, 1999). The error associated with larger scan angles is generally causing the outer beams, toward the swath edges, to attain a lower accuracy ~~(Guenther, 2007)~~(Guenther, 2007). This is a reason for the observed variations along the swath edges (Fig. ~~13~~12). Terrain slopes ~~has~~have the same effect of decreasing the vertical accuracy due to the footprint stretching. The measured ~~altitude tend~~elevation tends to be biased toward the shallowest point of the slope within the laser beam ~~(Guenther, 2007)~~(Guenther, 2007). However, the influence of slope is not crucial in the Knudedyb tidal inlet system, since it is generally a very flat area.

Vertical bias between overlapping swaths: Areas covered by more than a single swath tend to show more vertical variation in the LiDAR point measurements. This can be caused by variance/error in the GPS measurements and/or IMU errors ~~(Huising and Gomes Pereira, 1998)~~(Huising and Gomes Pereira, 1998). The vertical bias between swaths has been observed in the point cloud to be up to 5 cm, but it is varying throughout the study site. In most environments, a bias of 5 cm would be unnoticeable, but because of the large and very flat parts of the Knudedyb tidal inlet system, even a small bias becomes readily evident.

Water depth: The accuracy and precision are expected to be lower as the laser beam penetrates deeper into the water column ~~(Kunz et al., 1992)~~(Kunz et al., 1992). The laser beam footprint is diverging as it moves through the water column, resulting in a larger footprint on the seabed. The ~~altitude~~elevation of the detected point is thus derived from the measurement on a larger area on the seabed, which will decrease the vertical accuracy, as well as decrease the capability of detecting small objects. With this in mind, the ~~lower~~higher precision at the frame compared to the block is opposite of what would be expected, since the frame is below water and the block is on land. In this case, other factors, such as overlapping swaths and/or scan angle deviations, have more influence on the precision than the water depth. Also, it should be remembered that the frame surface was close to the water surface, and the effect of the water depth on the precision would most likely be more evident if it was located in deeper water.

Additional factors, beside the ones mentioned above, may influence the quality of LiDAR datasets. For instance, a dense vegetation cover of the seabed or breaking waves that makes the laser detection of the seabed almost impossible. However, these factors do not have a great influence in the studied part of the Knudedyb tidal inlet system, and thus they are not further elaborated.

5.5 Evaluation of the morphological classification

The morphological classification presented in this study is based on the studied section of the Knudedyb tidal inlet system. The overall concept of using tidal range, slope and variations of the ~~altitude~~elevation at different spatial scales proves to be a reliable method for delineating the morphological features in this tidal environment. The concept, however, can be applied in other environments. The specific thresholds in the classification determined in this study may deviate in other areas. Morphological features of different sizes require steps of other spatial scales in the neighbourhood analyses to produce a successful classification. In the future the classification method will be improved by implementing an objective method for determining the scales, which can make it applicable in areas with different morphological characteristics. ~~Such an objective scale determination method is presented by Ismail et al. (2015)~~Such an objective scale determination method is presented by Ismail et al. (2015), who determined the scales based on the variance of the DEM at progressively larger window sizes. In this way, the sizes of the morphological features are determining the scales for the classification.

5.6 Using topobathymetric LiDAR data to map morphology in a highly dynamic tidal environment

The study demonstrates the capability of green topobathymetric LiDAR to resolve fine-scale features, while covering a broad-scale tidal inlet system. Collecting topobathymetric LiDAR data with a high point density of 20 points/m^2 on average enables detailed seamless mapping of large tidal environments, and the LiDAR data has further proved to maintain a high accuracy. The combined characteristics of mapping with high resolution and high accuracy in a traditionally challenging environment provide many potential applications, such as mapping for purposes of spatial planning and management, safety of navigation, nature conservation, or morphological classification, as demonstrated in this study. The developed LiDAR data processing method is tailored to a morphological analysis application. The best representation of the morphology is mapped by gridding the average value of the LiDAR points into a DEM with a 0.5 × 0.5 resolution. Other applications would require different gridding techniques. For instance hydrographers, who are generally interested in mapping for navigational safety, would use the shallowest point for gridding. However, the overall method for processing the point cloud can be used regardless of the application. Only the last and least challenging/time consuming step of gridding the point cloud into a DEM, may vary depending on the application.

Applying topobathymetric LiDAR data for morphological analyses in tidal environments enables a holistic approach of seamlessly merging marine and terrestrial morphologies in a single dataset. ~~In~~However, a combination of topobathymetric LiDAR and MBES data is required, in order to map the morphology of tidal environments in full coverage~~, however, a combination of topobathymetric LiDAR and MBES swath data is required.~~. The comparable quality and resolution of LiDAR and MBES data gives a potential to map ~~large~~ broad-scale tidal environments, such as the Wadden Sea, in full coverage and with high resolution and high accuracy.

6 Conclusions

A~~ new~~ method was developed for processing raw topobathymetric Light Detection ~~a~~And Ranging (LiDAR) data into a ~~digital elevation model~~Digital Elevation Model (DEM) with seamless coverage across the land-water transition zone. ~~Specifically a procedure was developed for water surface detection utilizing automatic water level determination from only green LiDAR data in a tidal environment.~~ The method relies on basic principles, and ~~in general~~ the entire processing method is described with a high level of detail, which makes it transparent and easy to implement for future studies. Specifically a new procedure was developed for water surface detection in a tidal environment utilizing automatic water level determination solely based on green LiDAR data. The water surface detection method presented in this work did not take into account the variation in wave heights and surface slopes, which therefore constitutes a challenge to be addressed in future studies.

The vertical accuracy of the LiDAR data was determined by object detection of a cement block on land to ±8.1 cm with a 95% confidence level. The vertical precision was determined at the cement block to ±7.6 cm, and ±3.8 cm at a steel frame, placed just below the water surface. The horizontal mean error was determined at the block to ±10.4 cm. Overall, vertical and horizontal precision ~~is~~are within sub decimetre scale.

A seamless topobathymetric ~~digital elevation model~~DEM was created in a 4~~×~~ × 0.85 km section in the Knudedyb tidal inlet system. An average point density of 20 points per m^2 made it possible to create an elevation model of 0.5~~×~~ × 0.5 m resolution without significant interpolation. The ~~model extends~~DEM extended down to water depths of 3 m, which was determined as the maximum penetration depth of the laser scanning system at the given environmental conditions. Measurements of suspended sediment concentration and organic matter content ~~indicate~~indicated that the penetration depth ~~is~~was limited by the amount of organic matter rather than the amount of suspended sediment.

The vertical "dead zone" of the LiDAR data ~~has been~~was determined to ~~be~~ approx. 0-28 cm in the very shallow water.

The DEM was used as input in the Benthic Terrain Modeler tool to classify the study area into 5 classes of geomorphometry: broad-scale crests, fine-scale crests, depressions, slopes and flats. A morphological classification method was developed for classifying the area into 6 morphological classes: swash bars, linear bars, beach dunes, intertidal flats, intertidal creeks and subtidal channels. The morphological classification method ~~is~~was based on parameters of tidal range, terrain slope, a combination of various statistical neighbourhood analyses with varying window sizes and the area/perimeter-ratio of morphological features. The concept can be applied in any coastal environment with knowledge of the tidal range and the input of a ~~digital elevation model~~DEM; however, the thresholds may need adaptation, since they have been determined for the given study area. In the future the classification method should be improved by implementing an objective method for determining thresholds, which makes it immediately applicable across different environments.

Overall this study has demonstrated that airborne topobathymetric LiDAR is capable of seamless mapping across land-water transition zones even in environmentally challenging coastal environments with high water column turbidity and continuously varying water levels due to tides. Furthermore, we have demonstrated the potential of topobathymetric LiDAR in combination with morphometric analyses for classification of morphological features present in coastal land-water transition zones.

Acknowledgements

This work was funded by the Danish Council for Independent Research | Natural Sciences through the project "Process-based understanding and prediction of morphodynamics in a natural coastal system in response to climate change" (Steno Grant no. 10-081102) and by the Geocenter Denmark through the project "Closing the gap! – Coherent land-water environmental mapping (LAWA)" (Grant no. 4-2015).

References

Al-Hamdani, Z~~. K., Reker~~., Alanen, U., Andersen, J~~., Leth, J. O., Reijonen, A., Kotilainen, A.~~, H., Bekkby, T., Bendtsen, J., Bergström, U., Bučas, M., Carlén, I., Dahl, K., and ~~Dinesen, G. E.: Development of marine landscape maps for the~~Daunys, D.: Baltic Sea marine landscapes and ~~the Kattegat using geophysical~~habitats-mapping and ~~hydrographical parameters, Geological Survey of Denmark and Greenland Bulletin, 13, 61-64, 2007~~modeling, BALANCE Technical Summary Report, part 2/4, 2008.

Alexander, C.: Classification of Full-waveform Airborne Laser Scanning Data and Extraction of Attributes of Vegetation for Topographic Mapping, PhD Thesis, University of Leicester, 2010.

Allouis, T., Bailly, J. S., Pastol, Y., and Le Roux, C.: Comparison of LiDAR waveform processing methods for very shallow water bathymetry using Raman, near-infrared and green signals, Earth Surface Processes and Landforms, 35, 640-650, 2010.

~~Anderson, J. T., Van Holliday, D., Kloser, R., Reid, D. G., and Simard, Y.: Acoustic seabed classification: current practice and future directions, ICES Journal of Marine Science: Journal du Conseil, 65, 1004-1011, 2008.~~

Baltsavias, E. P.: Airborne laser scanning: basic relations and formulas, ISPRS Journal of Photogrammetry and Remote Sensing, 54, 199-214, 1999.

~~Bradbury, J.: A keyed classification of natural geodiversity for land management and nature conservation purposes, Proceedings of the Geologists' Association, 125, 329-349, http://dx.doi.org/10.1016/j.pgeola.2014.03.006, 2014.~~

Brzank, A., Heipke, C., Goepfert, J., and Soergel, U.: Aspects of generating precise digital terrain models in the Wadden Sea from lidar–water classification and structure line extraction, ISPRS Journal of Photogrammetry and Remote Sensing, 63, 510-528, 2008.

~~Carr-Betts, E., Beck, T. M., and Kraus, N. C.: Tidal Inlet Morphology Classification and Empirical Determination of Seaward and Down-Drift Extents of Tidal Inlets, Journal of Coastal Research, 28, 547-556, 10.2307/41508568, 2012.~~

Cavalli, M., and Marchi, L.: Characterisation of the surface morphology of an alpine alluvial fan using airborne LiDAR, Natural Hazards and Earth System Science, 8, 323-333, 2008.

Chauve, A., Mallet, C., Bretar, F., Durrieu, S., Deseilligny, M. P., and Puech, W.: Processing Full-Waveform LiDAR data: Modelling raw signals, Internatinal archives of Photogrammetry, Remote Sensing and Spatial Information Sciences, 2007.

Collin, A., Archambault, P., and Long, B.: Mapping the shallow water seabed habitat with the SHOALS, Geoscience and Remote Sensing, IEEE Transactions on, 46, 2947-2955, 2008.

Collin, A., Long, B., and Archambault, P.: Merging land-marine realms: Spatial patterns of seamless coastal habitats using a multispectral LiDAR, Remote Sensing of Environment, 123, 390-399, 2012.

~~DCA (Danish Coastal Authority):~~DCA: Wave data - Fanø Bugt, http://kysterne.kyst.dk/pages/10852/waves/showData.asp?targetDay=30-05-2014&ident=3071&subGroupGuid=16406, last access: 9 March 2016, 2014.

~~De Swart, H., and Zimmerman, J.: Morphodynamics of tidal inlet systems, Annual Review of Fluid Mechanics, 41, 203-229, 2009.~~

Diesing, M., Coggan, R., and Vanstaen, K.: Widespread rocky reef occurrence in the central English Channel and the implications for predictive habitat mapping, Estuarine, Coastal and Shelf Science, 83, 647-658, 2009.

Dix, M., Abd-Elrahman, A., Dewitt, B., and Nash, L.: Accuracy Evaluation of Terrestrial LIDAR and Multibeam Sonar Systems Mounted on a Survey Vessel, Journal of Surveying Engineering, 138, 203-213, 10.1061/(ASCE)SU.1943-5428.0000075, 2012.

~~DMI (Danish Meteorological Institute):~~DMI: Vejr- og klimadata, Danmark - Ugeoversigt 2014 - 22, 26 Maj 2014 - 1 Juni 2014, http://www.dmi.dk/uploads/tx_dmidatastore/webservice/t/g/i/s/r/20140601ugeoversigt.pdf, last access: 9 March 2016, 2014.

Doneus, M., Doneus, N., Briese, C., Pregesbauer, M., Mandlburger, G., and Verhoeven, G.: Airborne laser bathymetry–detecting and recording submerged archaeological sites from the air, J Archeol Sci, 40, 2136-2151, 2013.

Ernstsen, V. B., Noormets, R., Hebbeln, D., Bartholomä, A., and Flemming, B. W.: Precision of high-resolution multibeam echo sounding coupled with high-accuracy positioning in a shallow water coastal environment, Geo-mar lett, 26, 141-149, ~~2006a~~2006.

~~Ernstsen, V. B., Noormets, R., Winter, C., Hebbeln, D., Bartholomä, A., Flemming, B. W., and Bartholdy, J.: Quantification of dune dynamics during a tidal cycle in an inlet channel of the Danish Wadden Sea, Geo-Marine Letters, 26, 151-163, 2006b.~~

~~Finkl, C. W., Benedet, L., and Andrews, J. L.: Interpretation of seabed geomorphology based on spatial analysis of high-density airborne laser bathymetry, Journal of Coastal Research, 501-514, 2005.~~

~~FitzGerald, D., Buynevich, I., and Hein, C.: Morphodynamics and facies architecture of tidal inlets and tidal deltas, in: Principles of Tidal Sedimentology, Springer, 301-333, 2012.~~

Graham, L.: Accuracy. Precision and all That Jazz, LiDAR Magazine, 2, 2012.

Guenther, G. C.: Airborne laser hydrography: System design and performance factors, DTIC Document, 1985.

Guenther, G. C., Cunningham, A. G., LaRocque, P. E., and Reid, D. J.: Meeting the accuracy challenge in airborne lidar bathymetry, EARSel, Dresden, 2000.

Guenther, G. C.: Airborne lidar bathymetry, Digital elevation model technologies and applications: The DEM users manual, 2, 253-320, 2007.

Hladik, C., and Alber, M.: Accuracy assessment and correction of a LIDAR-derived salt marsh digital elevation model, Remote Sens Environ, 121, 224-235, 2012.

Hofle, B., Vetter, M., Pfeifer, N., Mandlburger, G., and Stotter, J.: Water surface mapping from airborne laser scanning using signal intensity and elevation data, Earth Surface Processes and Landforms, 34, 1635, 2009.

Hogg, O. T., Huvenne, V. A., Griffiths, H. J., Dorschel, B., and Linse, K.: Landscape mapping at sub-Antarctic South Georgia provides a protocol for underpinning large-scale marine protected areas, Scientific Reports, 6, 33163, 2016.

Huising, E. J., and Gomes Pereira, L. M.: Errors and accuracy estimates of laser data acquired by various laser scanning systems for topographic applications, ISPRS Journal of Photogrammetry and Remote Sensing, 53, 245-261, http://dx.doi.org/10.1016/S0924-2716(98)00013-6, 1998.

Höfle, B., and Rutzinger, M.: Topographic airborne LiDAR in geomorphology: A technological perspective, Zeitschrift für Geomorphologie, Supplementary Issues, 55, 1-29, 2011.

IHO: IHO Standards for Hydrographic Surveys (S-44), 5th edition, International Hydrographic Bureau Monaco, 2008.

Ismail, K., Huvenne, V. A., and Masson, D. G.: Objective automated classification technique for marine landscape mapping in submarine canyons, Marine Geology, 362, 17-32, 2015.

Jensen, J. R.: Remote sensing of the environment: An earth resource perspective 2/e, Pearson Education India, 2009.

Kaskela, A. M., Kotilainen, A. T., Al-Hamdani, Z., Leth, J. O., and Reker, J.: Seabed geomorphic features in a glaciated shelf of the Baltic Sea, Estuarine, Coastal and Shelf Science, 100, 150-161, http://dx.doi.org/10.1016/j.ecss.2012.01.008, 2012.

Klagenberg, P. A., Knudsen, S. B., Sørensen, C., and Sørensen, P.: Morfologisk udvikling i Vadehavet: Knudedybs tidevandsområde, Kystdirektoratet, 2008.

Klemas, V.: Airborne remote sensing of coastal features and processes: An overview, J Coastal Res, 29, 239-255, 2013.

Kunz, G., Lamberts, C., van Mierlo, G., de Vries, F., Visser, H., Smorenburg, C., Spitzer, D., and Hofstraat, H.: Laser bathymetry in the Netherlands, EAR-SeL Advances in Remote Sensing, 36-41, 1992.

Lecours, V., Dolan, M. F. J., Micallef, A., and Lucieer, V. L.: A review of marine geomorphometry, the quantitative study of the seafloor, Hydrol. Earth Syst. Sci., 20, 3207-3244, 10.5194/hess-20-3207-2016, 2016.

Lefebvre, A., Ernstsen, V. B., and Winter, C.: Estimation of roughness lengths and flow separation over compound bedforms in a natural-tidal inlet, Cont Shelf Res, 61-62, 98-111, 10.1016/j.csr.2013.04.030, 2013.

Leica: Leica LiDAR Survey Studio flyer, available at: http://leica-geosystems.com/products/airborne-systems/software/leica-lidar-survey-studio, last access: 24 March 2016, Heerbrugg, Switzerland, 2015.

Lundblad, E. R., Wright, D. J., Miller, J., Larkin, E. M., Rinehart, R., Naar, D. F., Donahue, B. T., Anderson, S. M., and Battista, T.: A benthic terrain classification scheme for American Samoa, Marine Geodesy, 29, 89-111, 2006.

Mallet, C., and Bretar, F.: Full-waveform topographic lidar: State-of-the-art, ISPRS J Photogramm, 64, 1-16, 2009.

Mandlburger, G., Pfennigbauer, M., Steinbacher, F., and Pfeifer, N.: Airborne Hydrographic LiDAR Mapping-Potential of a new technique for capturing shallow water bodies, Proceedings of ModSim'11, 2011.

Mandlburger, G., Pfennigbauer, M., and Pfeifer, N.: Analyzing near water surface penetration in laser bathymetry-A case study at the River Pielach, ISPRS Annals of Photogrammetry, Remote Sensing and Spatial Information Sciences, 1, 175-180, 2013.

Mandlburger, G., Hauer, C., Wieser, M., and Pfeifer, N.: Topo-bathymetric LiDAR for monitoring river morphodynamics and instream habitats—A case study at the Pielach River, Remote Sensing, 7, 6160-6195, 2015.

Millard, R. C., and Seaver, G.: An index of refraction algorithm for seawater over temperature, pressure, salinity, density, and wavelength, Deep Sea Research Part A.

Oceanographic Research Papers, 37, 1909-1926, http://dx.doi.org/10.1016/0198-0149(90)90086-B, 1990.

Mousavi, M., Irish, J., Frey, A., Olivera, F., and Edge, B.: Global warming and hurricanes: the potential impact of hurricane intensification and sea level rise on coastal flooding, Climatic Change, 104, 575-597, 10.1007/s10584-009-9790-0, 2011.

Nayegandhi, A., Brock, J., and Wright, C.: Small-footprint, waveform-resolving lidar estimation of submerged and sub-canopy topography in coastal environments, Int J Remote Sens, 30, 861-878, 2009.

Niemeyer, J., and Soergel, U.: Opportunities of Airborne Laser Bathymetry for the Monitoring of the Sea Bed on the Baltic Sea Coast, ISPRS J Photogramm, Remote Sensing and Spatial Information Sciences, 1, 179-184, 2013.

Optech: Optech HydroFusion Information Sheet, available at: http://www.teledyneoptech.com/wp-content/uploads/specification_hydrofusion.pdf, last access: 24 March 2016, Canada, 2013.

Parker, H., and Sinclair, M.: The successful application of Airborne LiDAR Bathymetry surveys using latest technology, OCEANS, 2012 - Yeosu, 2012, 1-4,

~~Pastol, Y., Le Roux, C., and Louvart, L.: LITTO D-A Seamless Digital Terrain Model, The International hydrographic review, 8, 2007.~~

Pe'eri, S., and Long, B.: LIDAR technology applied in coastal studies and management, J Coastal Res, 1-5, 2011.

Pedersen, J. B. T., and Bartholdy, J.: Budgets for fine-grained sediment in the Danish Wadden Sea, Mar Geol, 235, 101-117, 2006.

Pike, R., Evans, I., and Hengl, T.: Geomorphometry: a brief guide, Developments in Soil Science, 33, 3-30, 2009.

RIEGL: LAS extrabytes implementation in RIEGL software - Whitepaper, RIEGL Laser Measurement Systems GmbH, available at: www.riegl.com/uploads/tx_pxpriegldownloads/Whitepaper_-_LAS_extrabytes_implementation_in_Riegl_software_01.pdf, last access: 24 March 2016, 2012.

RIEGL: Datasheet RIEGL VQ-820-G, RIEGL Laser Measurement Systems GmbH, available at: http://www.riegl.com/uploads/tx_pxpriegldownloads/DataSheet_VQ-820-G_2015-03-24.pdf, last access: 24 March 2016, 2014.

RIEGL: Data Sheet RiHYDRO, RIEGL Laser Measurement Systems GmbH, available at: http://www.riegl.com/uploads/tx_pxpriegldownloads/11_DataSheet_RiHYDRO_2015-08-24_01.pdf, last access: 24 March 2016, 2015.

Rinehart, R., Wright, D. J., Lundblad, E. R., Larkin, E. M., Murphy, J., and Cary-Kothera, L.: ArcGIS 8. x benthic terrain modeler: Analysis in American Samoa, Proceedings of the 24th Annual ESRI User Conference, San Diego, CA, Paper, 2004, 2004,

Sacchetti, F., Benetti, S., Georgiopoulou, A., Dunlop, P., and Quinn, R.: Geomorphology of the Irish Rockall Trough, North Atlantic Ocean, mapped from multibeam bathymetric and backscatter data, Journal of Maps, 7, 60-81, 2011.

Schmidt, A., Rottensteiner, F., and Soergel, U.: Classification of airborne laser scanning data in Wadden sea areas using conditional random fields, International Archives of the Photogrammetry, Remote Sensing and Spatial Information Sciences XXIX-B3, 161-166, 2012.

Steinbacher, F., Pfennigbauer, M., Aufleger, M., and Ullrich, A.: High resolution airborne shallow water mapping, International Archives of the Photogrammetry, Remote Sensing and Spatial Information Sciences, Proceedings of the XXII ISPRS Congress, 2012,

Su, L., and Gibeaut, J.: EXTRACTING SURFACE FEATURES OF THE NUECES RIVER DELTA USING LIDAR POINTS, ASPRS/MAPPS 2009 Fall Conference, San Antonio, Texas, November 16-19, 2009.

Verfaillie, E., Doornenbal, P., Mitchell, A. J., White, J., and Van Lancker, V.: The bathymetric position index (BPI) as a supprt tool for habitat mapping. Worked example for the MESH Final Guidance, 14 pp., 2007.

Wang, C.-K., and Philpot, W. D.: Using airborne bathymetric lidar to detect bottom type variation in shallow waters, Remote Sensing of Environment, 106, 123-135, 2007.

Wright, D., Lundblad, E., Larkin, E., Rinehart, R., Murphy, J., Cary-Kothera, L., and Draganov, K.: ArcGIS Benthic Terrain Modeler, Corvallis, Oregon, Oregon State University, Davey Jones Locker Seafloor Mapping/Marine GIS Laboratory and NOAA Coastal Services Center, Accessible online at: http://www. csc. noaa. gov/products/btm, 2005.

Table 1: Vertical accuracy and precision of the LiDAR point measurements, in terms of minimum error (E_{min}), maximum error (E_{max}), standard deviation (σ), mean absolute error (E_{MA}), root mean square error (E_{RMS}) and the 95% confidence level ($Cl_{95\%}$).

Accuracy/ Precision	Object	Best-fit plane	# points n	E_{min} (cm)	E_{max} (cm)	σ (cm)	E_{MA} (cm)	E_{RMS} (cm)	$Cl_{95\%}$ (cm)
Accuracy	Cement block	GCPs	227	0.01	12.1	4.1	3.5	±4.1	±8.1
Precision	Cement block	Point cloud	227	0.04	12.9	3.9	2.8	±3.9	±7.6
Precision	Steel frame	Point cloud	46	0.02	5.5	2.0	1.6	±1.9	±3.8

Table 2: LiDAR point spacing and density for all the 11 individual swaths, which covered the study area, and for the combined swaths.

Swath number	1	2	3	4	5	6	7	8	9	10	11	All
Point spacing (m)	0.30	0.30	0.36	0.31	0.36	0.32	0.37	0.29	0.35	0.36	0.28	0.20
Point density (pt./m^2)	10.8	10.8	7.8	10.2	7.5	9.6	7.2	11.7	8.0	7.8	12.7	19.6

1

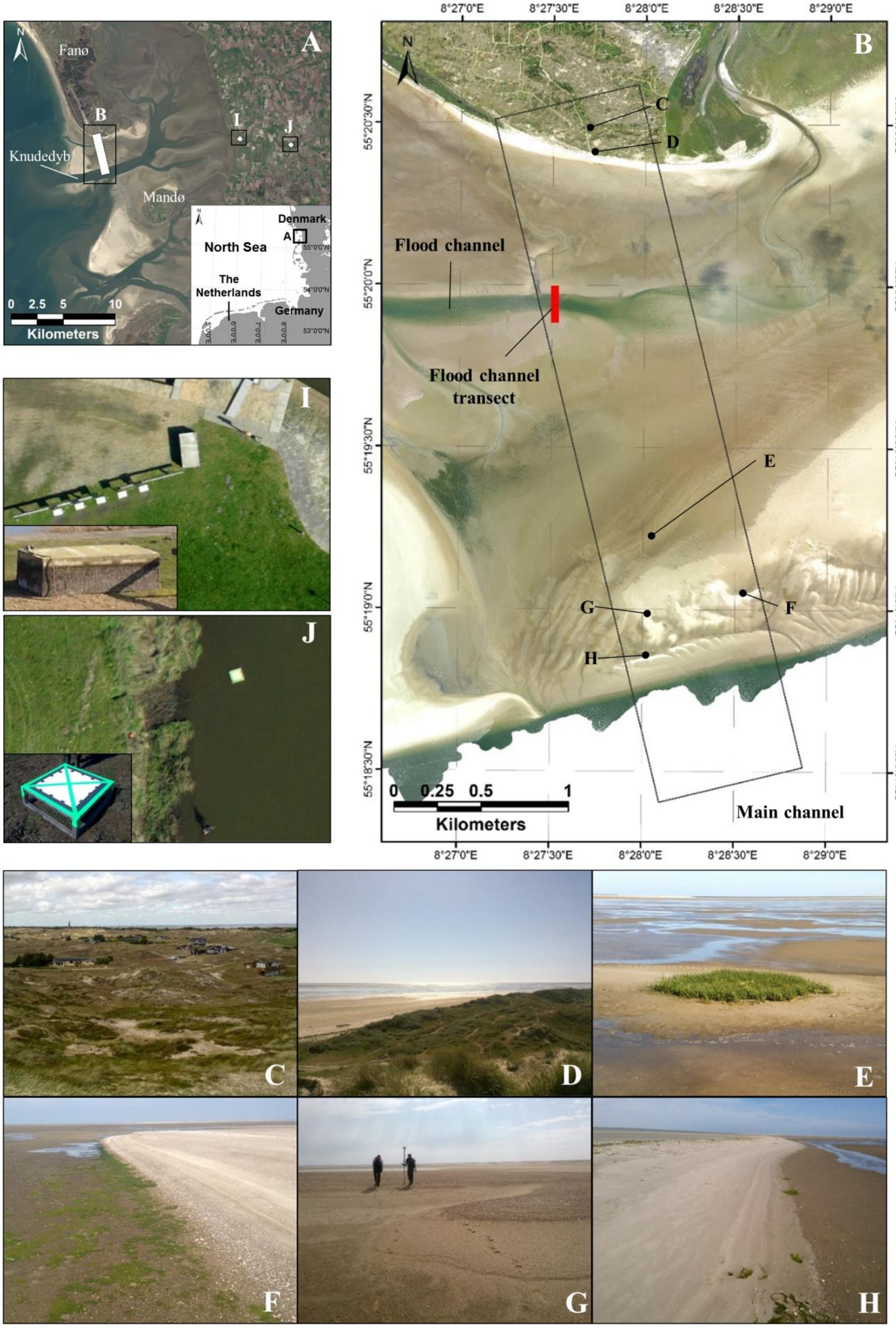
Fanø
A
B
Knudedyb
I
J
Mandø
Denmark
A
North Sea
The Netherlands
Germany
0 2.5 5 10
Kilometers
8°27'0"E
8°27'30"E
8°28'0"E
8°28'30"E
8°29'0"E
55°20'30"N
55°20'0"N
55°19'30"N
55°19'0"N
55°18'30"N
C
D
Flood channel
Flood channel transect
E
G
F
H
0 0.25 0.5 1
Kilometers
Main channel
I
J
C
D
E
F
G
H

Figure ~~2~~1: A) Overview of the study area location in the Danish Wadden Sea and the specific locations of the study site (B) and the two validation sites (I and J) (22 April 2015 satellite image, Landsat 8). B) The study site in the Knudedyb tidal inlet system (30 May 2015 Orthophoto, AHM). C) Cottages in the dunes on Fanø. D) Beach dunes on Fanø. E) Patch of *Spartina Townsendii* (Common Cord Grass). F-G) Swash bars. H) Linear bar. I) Validation site 1 with a cement block on land, used for accuracy and precision assessment (19 April 2015 orthophoto, AHM). J) Validation site 2 with a steel frame in Ribe Vesterå River, used for precision assessment (19 April 2015 orthophoto, AHM).

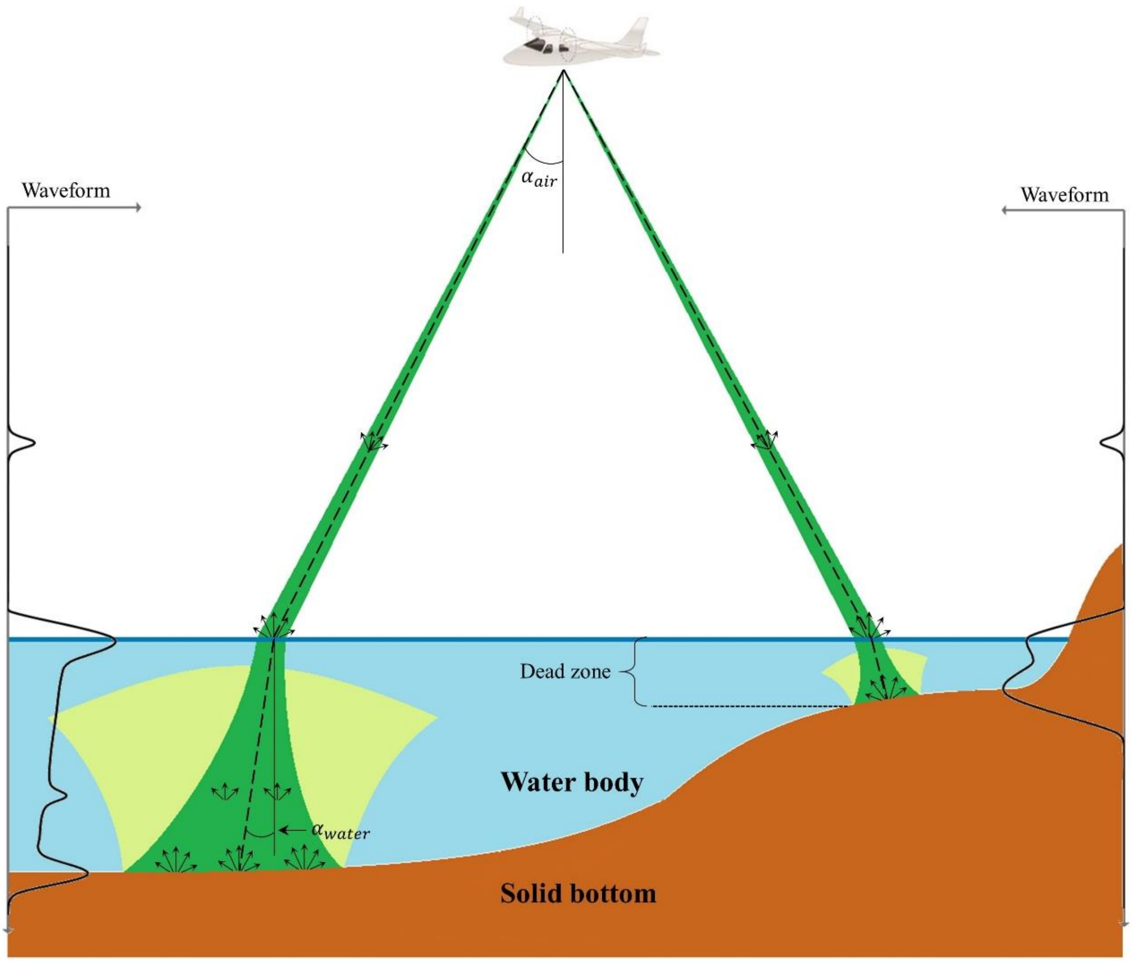

Figure 2~~1~~: Conceptual sketch of the laser beam propagation and return signals. The beam refracts upon entering the water body, and it diverges as it propagates through the water column. Return signals are produced both in the air, at the water surface, in the water column and at the seabed. The LiDAR instrument has limited capability in very shallow water (the "dead zone" in the figure) because the successive peaks from the water surface and the seabed are not individually separated in time and amplitude. Only the largest peak, which is from the seabed, is detected.

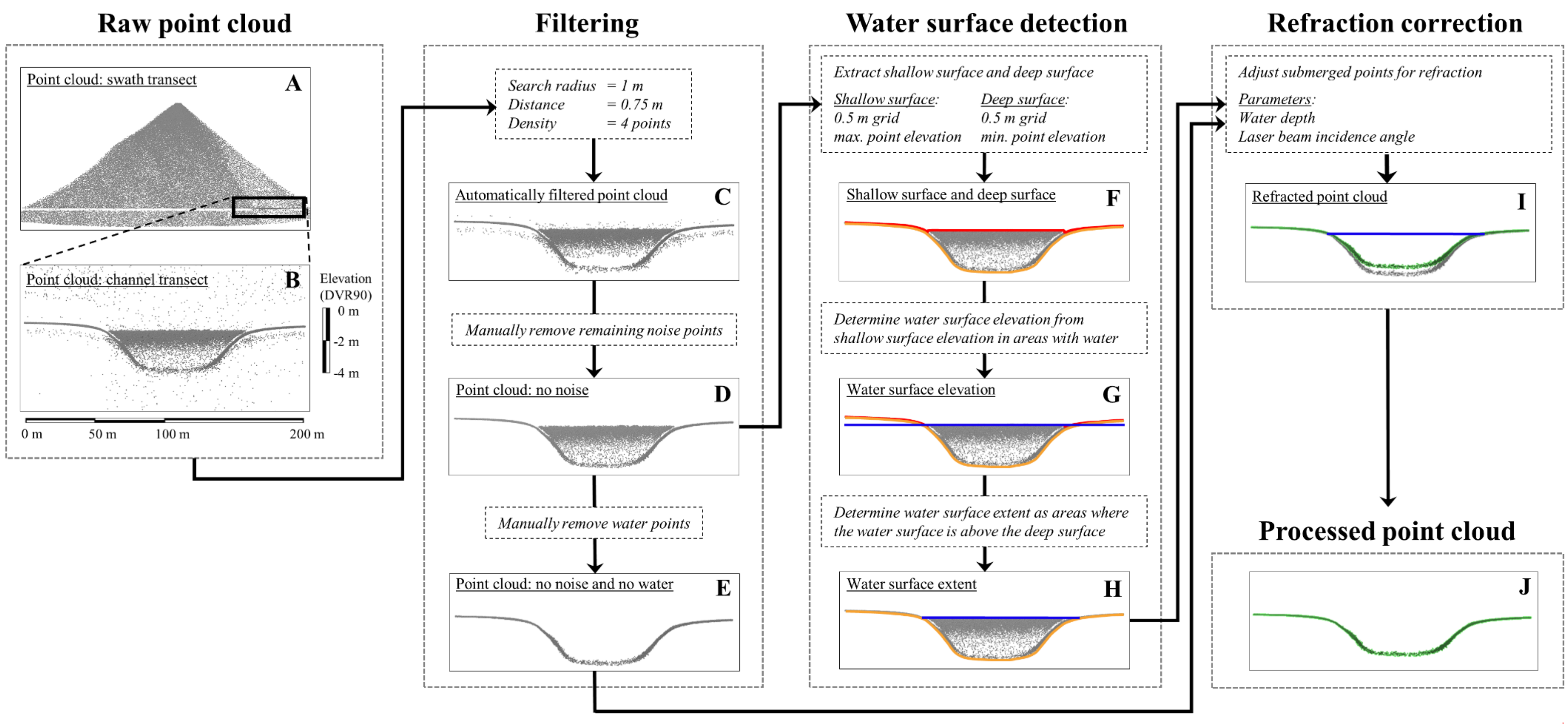

Figure 3: Workflow for processing the LiDAR point cloud. A) Point cloud from a single swath with points ranging from -100 m to 300 m elevation. B) Zoom-in on a cross section of the flood channel with ~~altitudes~~elevationselevation exaggerated ×15 for visualization purpose. C-E) Method for filtering the point cloud. F-H) Method for detecting a water surface (blue) based on the extraction of a shallow surface (red) and a deep surface (orange). I) Correction for the effect of refraction on all the submerged points. J) Processed point cloud

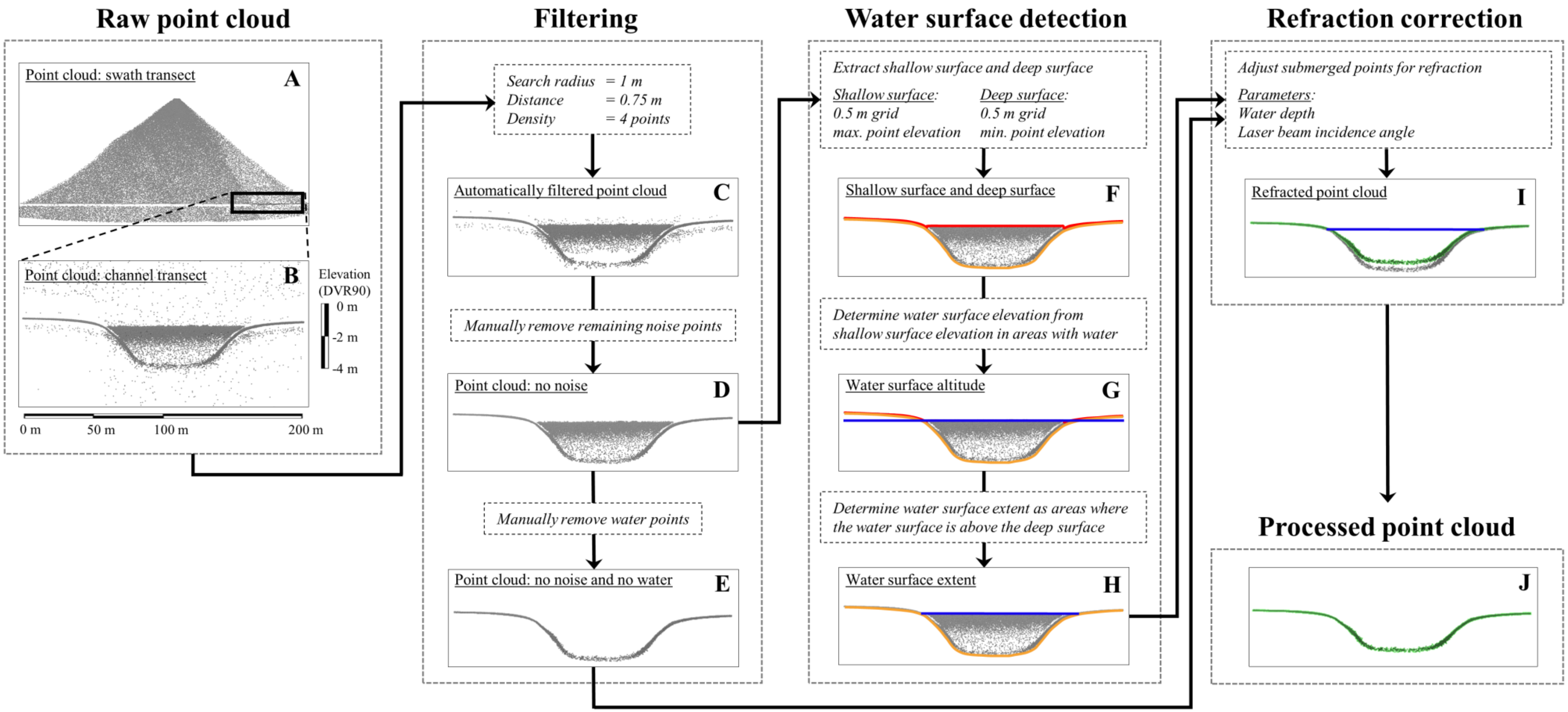
Raw point cloud
Point cloud: swath transect
A
Point cloud: channel transect
B
Elevation
(DVR90)
0 m
-2 m
-4 m
0 m
50 m
100 m
200 m
Filtering
Search radius = 1 m
Distance = 0.75 m
Density = 4 points
Automatically filtered point cloud
C
Manually remove remaining noise points
Point cloud: no noise
D
Manually remove water points
Point cloud: no noise and no water
E
Water surface detection
Extract shallow surface and deep surface
Shallow surface:
0.5 m grid
max. point elevation
Deep surface:
0.5 m grid
min. point elevation
Shallow surface and deep surface
F
Determine water surface elevation from shallow surface elevation in areas with water
Water surface altitude
G
Determine water surface extent as areas where the water surface is above the deep surface
Water surface extent
H
Refraction correction
Adjust submerged points for refraction
Parameters:
Water depth
Laser beam incidence angle
Refracted point cloud
I
Processed point cloud
J

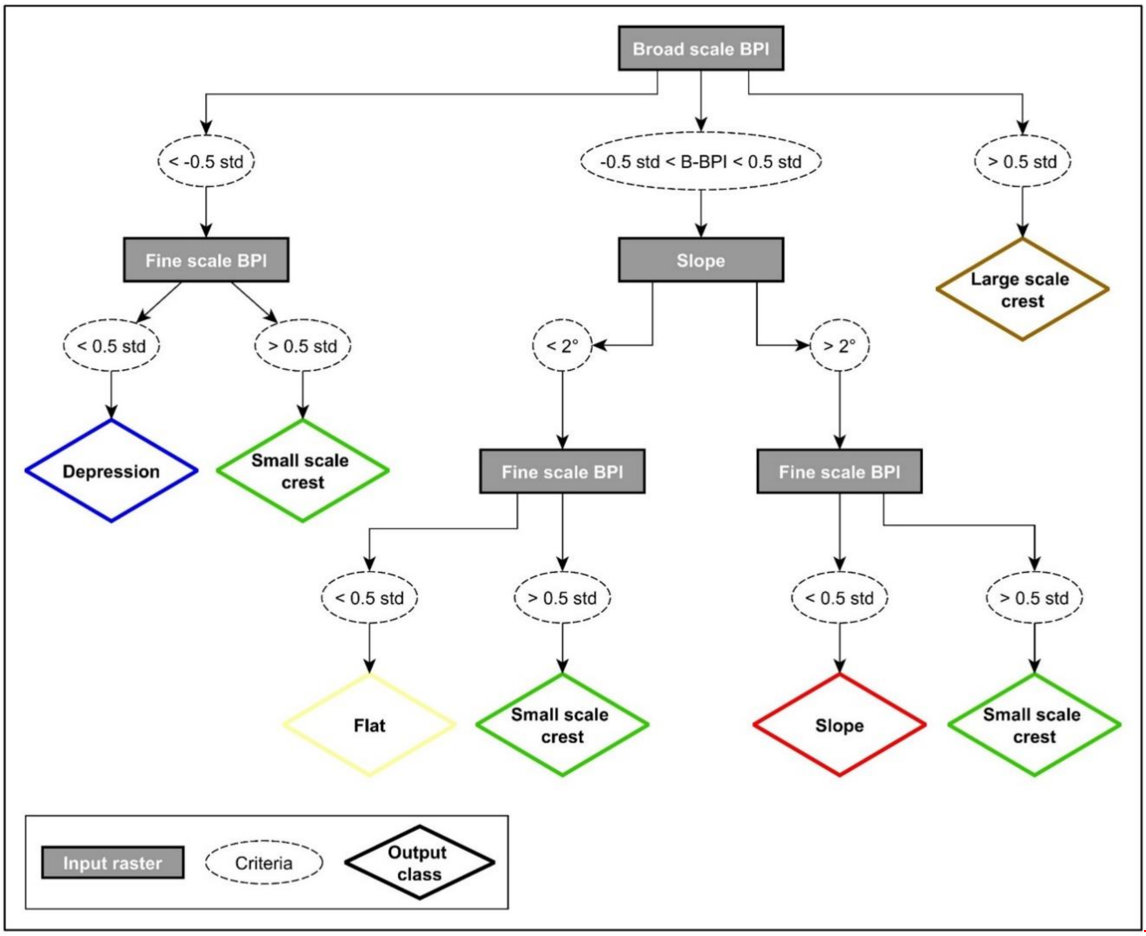
Broad scale BPI
< -0.5 std
-0.5 std < B-BPI < 0.5 std
> 0.5 std
Fine scale BPI
Slope
Large scale crest
< 0.5 std
> 0.5 std
< 2°
> 2°
Depression
Small scale crest
Fine scale BPI
Fine scale BPI
< 0.5 std
> 0.5 std
< 0.5 std
> 0.5 std
Flat
Small scale crest
Slope
Small scale crest
Input raster
Criteria
Output class

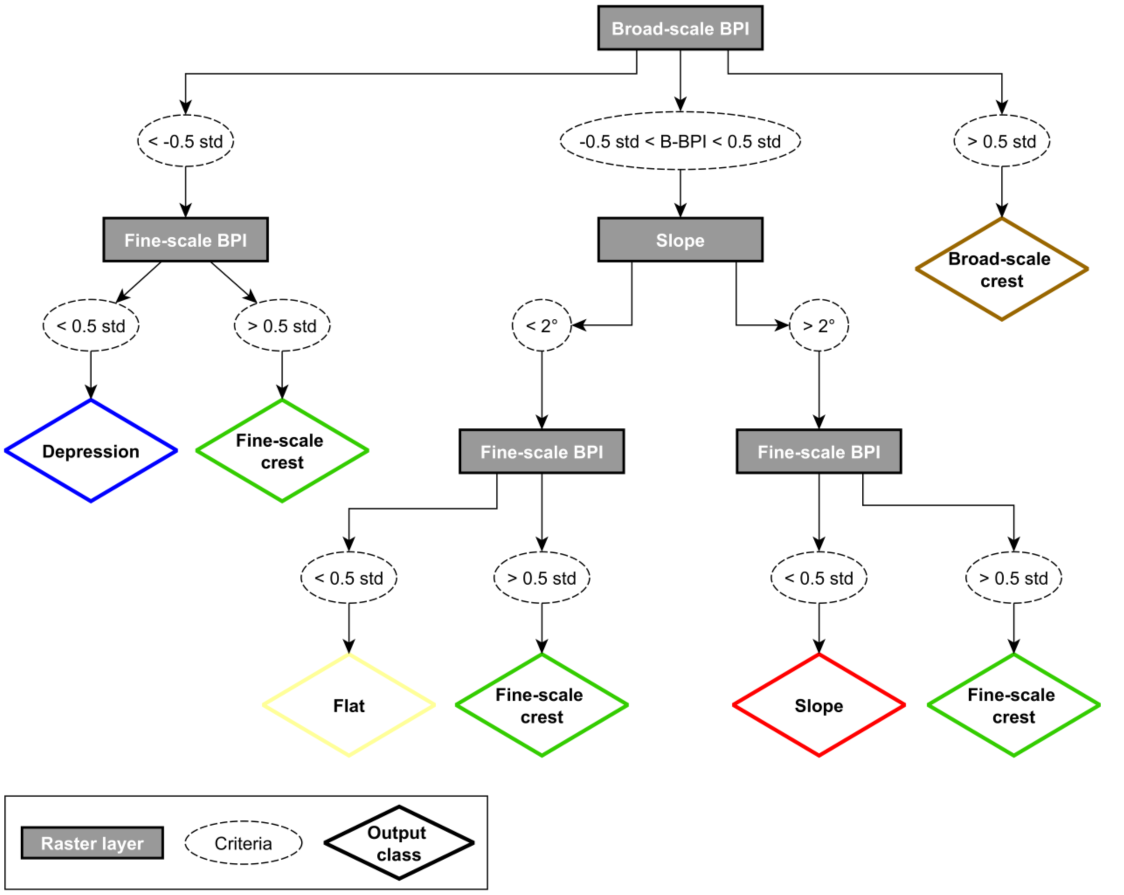

Figure 4: Classification decision tree, showing how the geomorphometric classification was conducted in the Benthic Terrain Model tool.

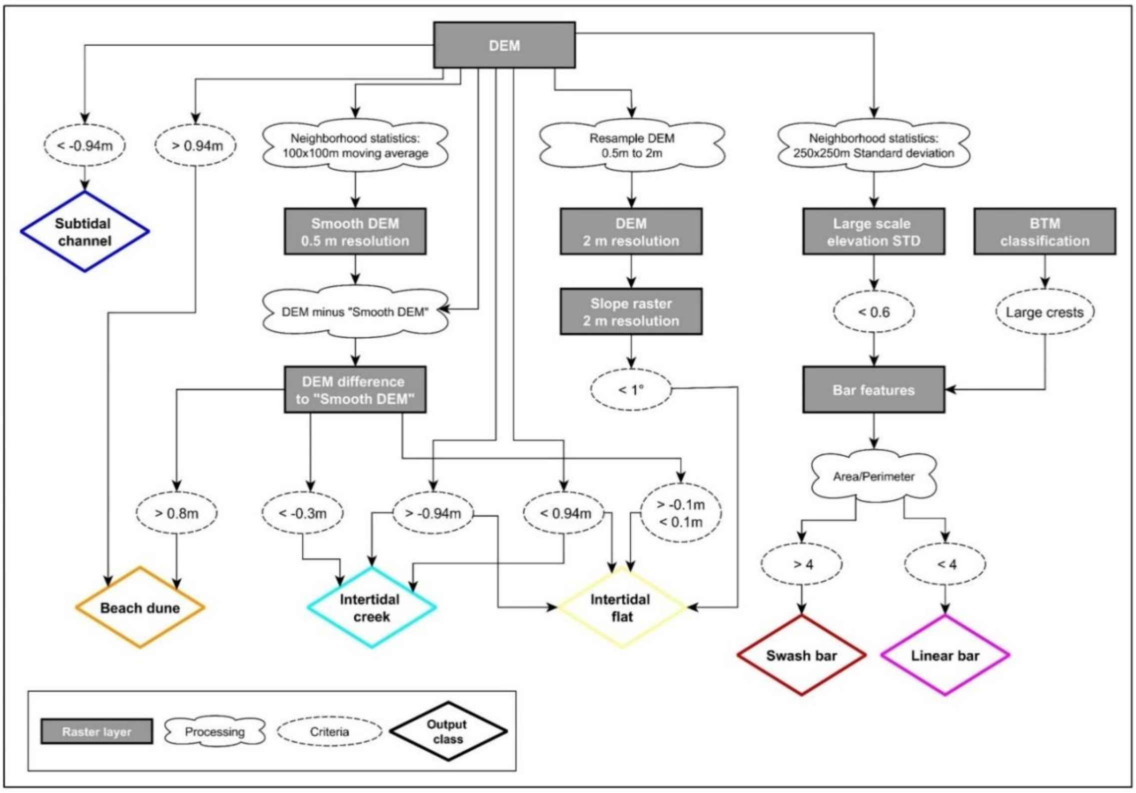

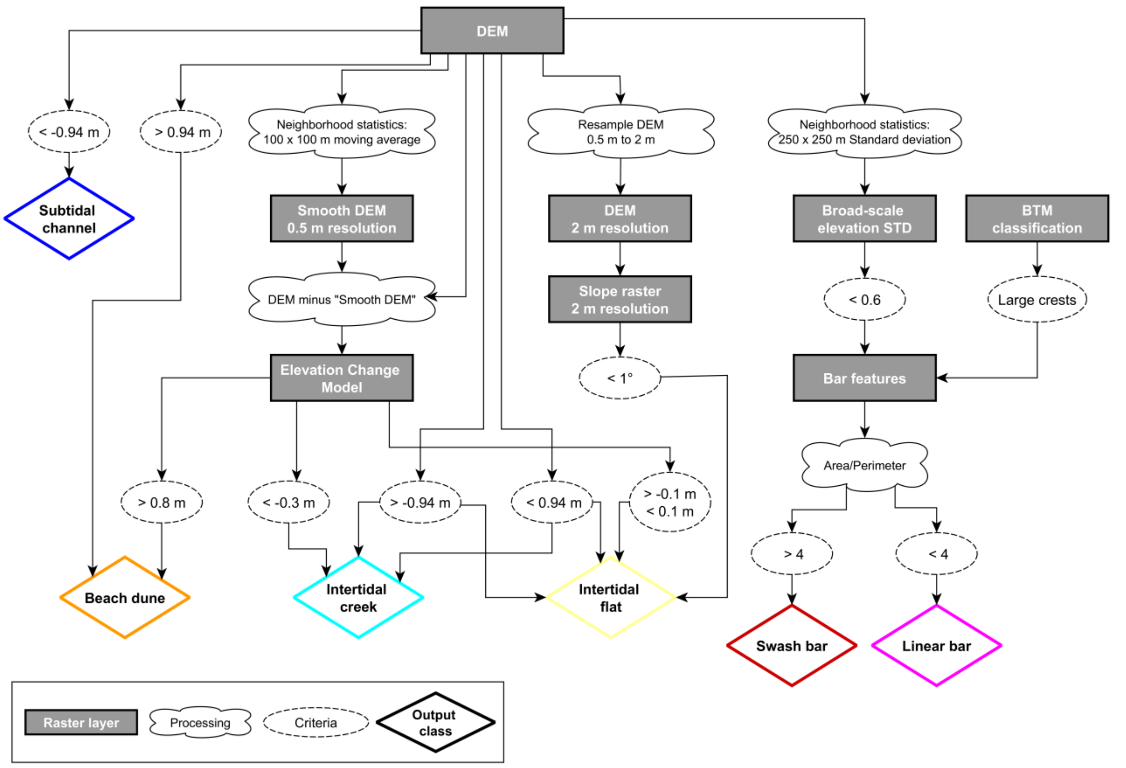

Figure 5: Classification decision tree of the morphological classification. All steps were performed in ArcGIS.

1

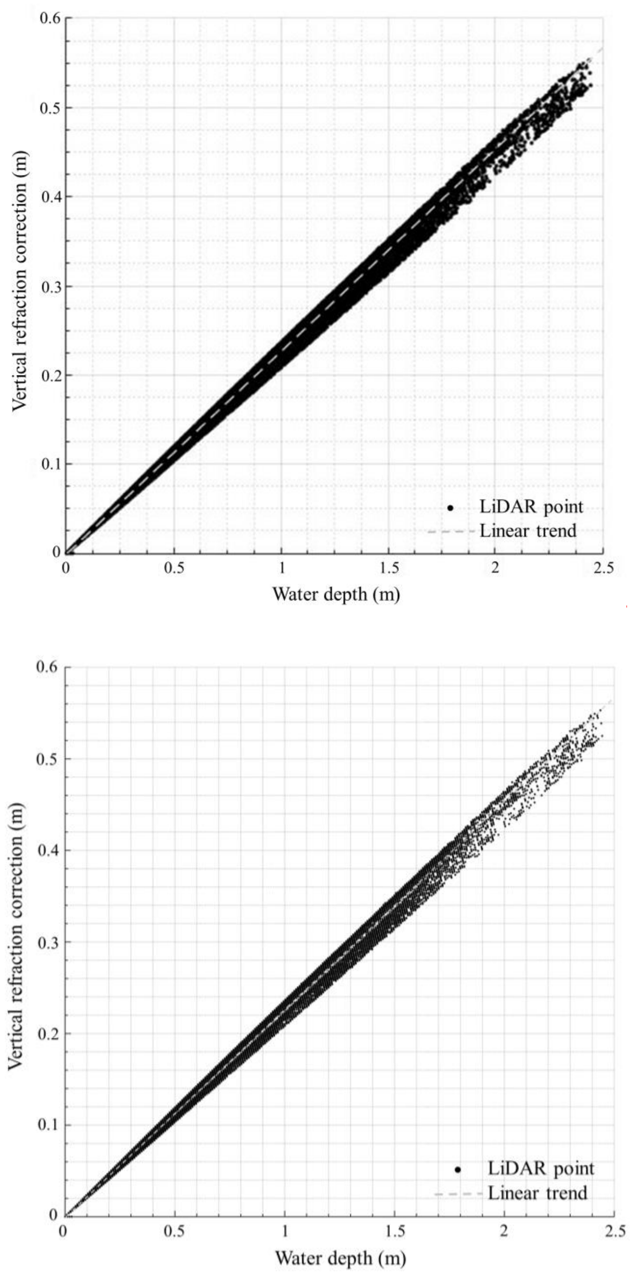

Figure 6: Vertical adjustment of the refracted LiDAR points from the flood channel transect (see location in Fig. ~~2C~~1B).

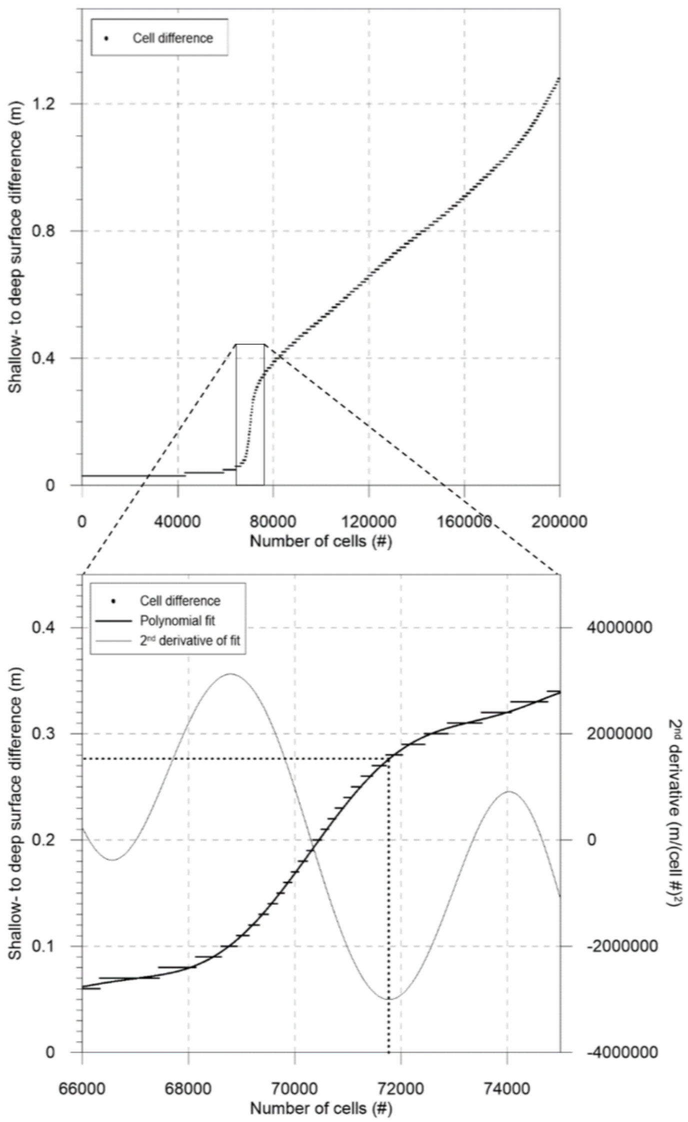

Figure 7: Vertical difference between the shallowest and the deepest LiDAR point within 0.5 m grid cells in the land-water transition zone. -The abrupt change is caused by the dead zone. The vertical extent of the dead zone is determined to approx. 28 cm, derived by the maximum rate of change of a polynomial fit through the points.

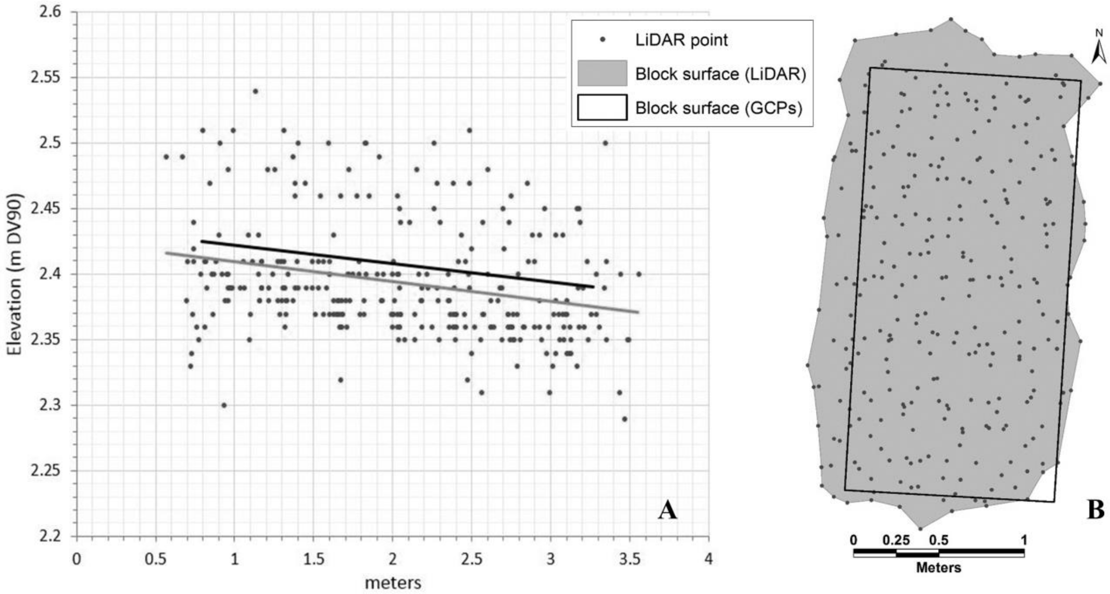

Figure 8: Vertical and horizontal distribution of the LiDAR points describing the block surface and the actual block surface derived from ~~Ground Control Points (~~GCPs~~).~~. A) LiDAR points (grey dots) compared to the GCP block surface (black line) for determining the vertical accuracy. The grey line shows the LiDAR block surface as a best-linear-fit through the points. B) Block surface derived from the four GCP corner points and the block surface derived by the perimeter of the LiDAR points.

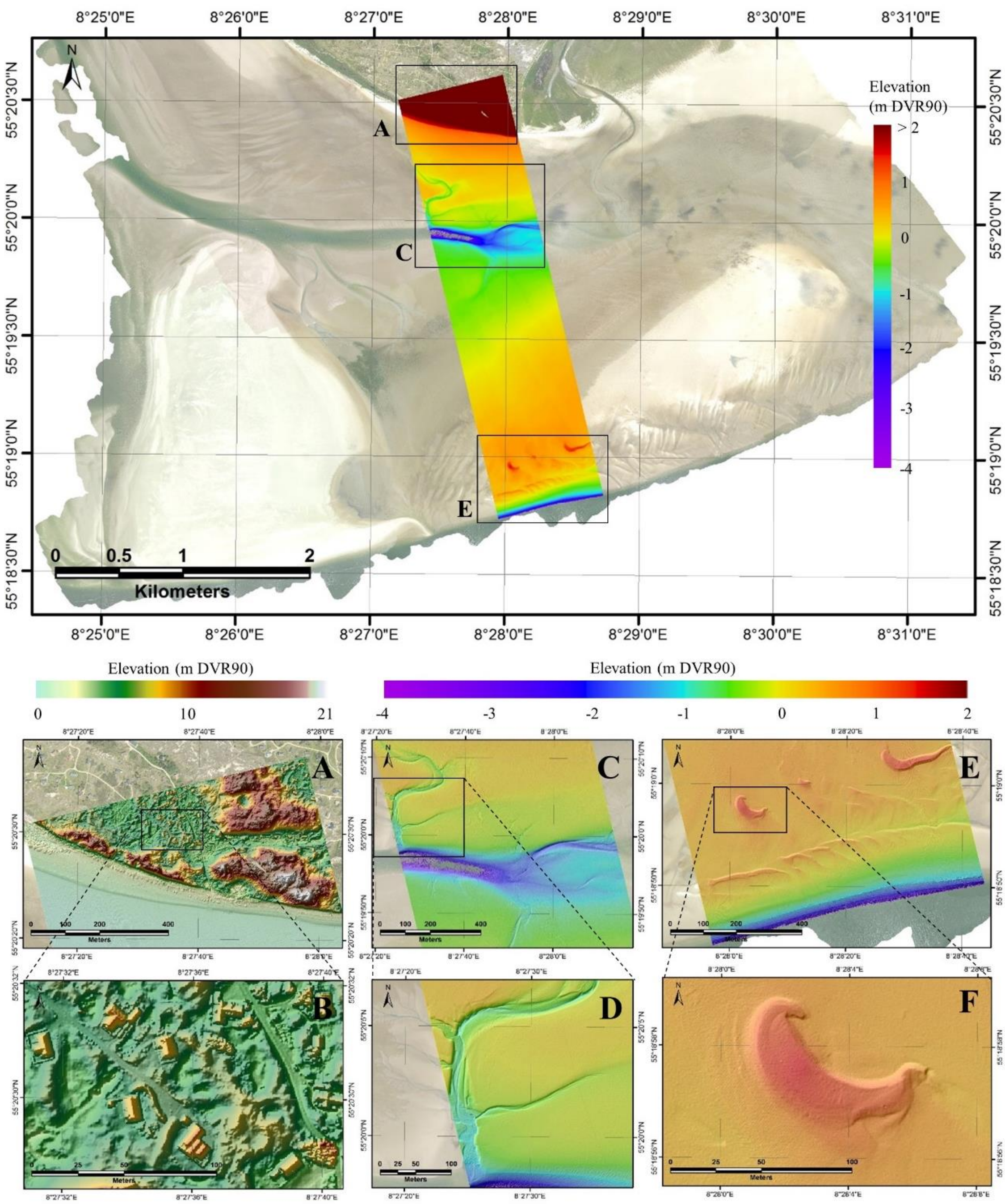

8°25'0"E
8°26'0"E
8°27'0"E
8°28'0"E
8°29'0"E
8°30'0"E
8°31'0"E
55°20'30"N
55°20'0"N
55°19'30"N
55°19'0"N
55°18'30"N
Elevation
(m DVR90)
> 2
1
0
-1
-2
-3
-4
A
C
E
0
0.5
1
2
Kilometers
Elevation (m DVR90)
0
10
21
Elevation (m DVR90)
-4
-3
-2
-1
0
1
2
A
B
C
D
E
F
Meters

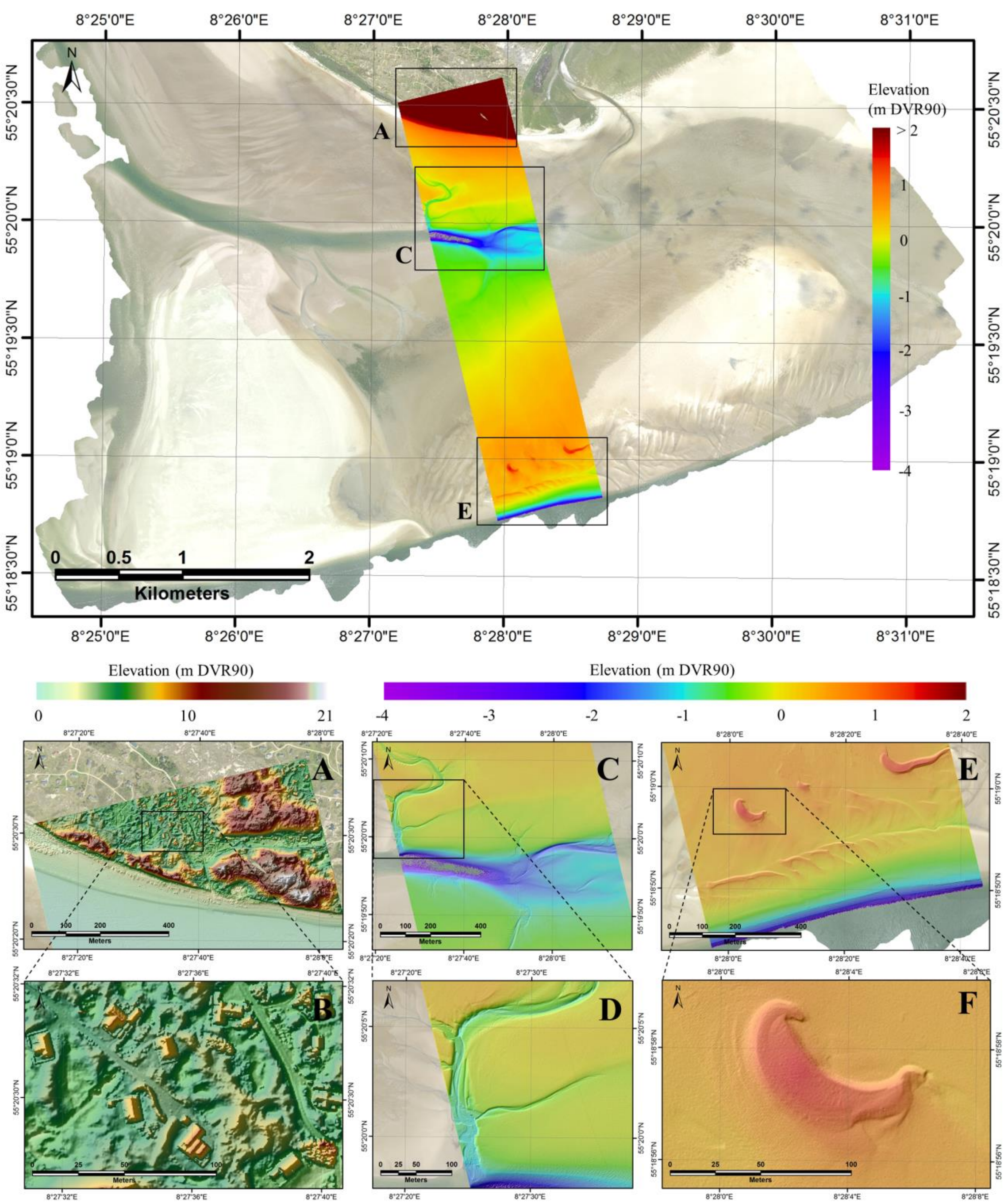

Figure 9: Topobathymetric DEM across the northern part of the Knudedyb tidal inlet system with close-up views of different detail level ~~on~~in specific areas. The northern supratidal part of the study area (A ~~hill shade is draped upon the close-ups for improved visualization of morphological features. A) Northern section with~~and B) includes beach dunes, vegetation and cottages~~.~~, thus~~ B) Cottages. C) Mid-section with~~ the ~~flood channel. D) Closer view on an~~DEM can be regarded as a DSM in this specific section. In the sub- and intertidal parts of the study area (C, D, E and F), the DEM reflects the

natural terrain, thus it can be regarded as a DTM. A) Beach dunes, vegetation and cottages. B) Cottages. C) Flood channel. D) Intertidal creek. E) ~~Southern section with swash~~Swash bars, linear bars and bathymetry of the main channel. F) Swash bar. A hillshade is draped upon the close-up views for improved visualization of morphological features.

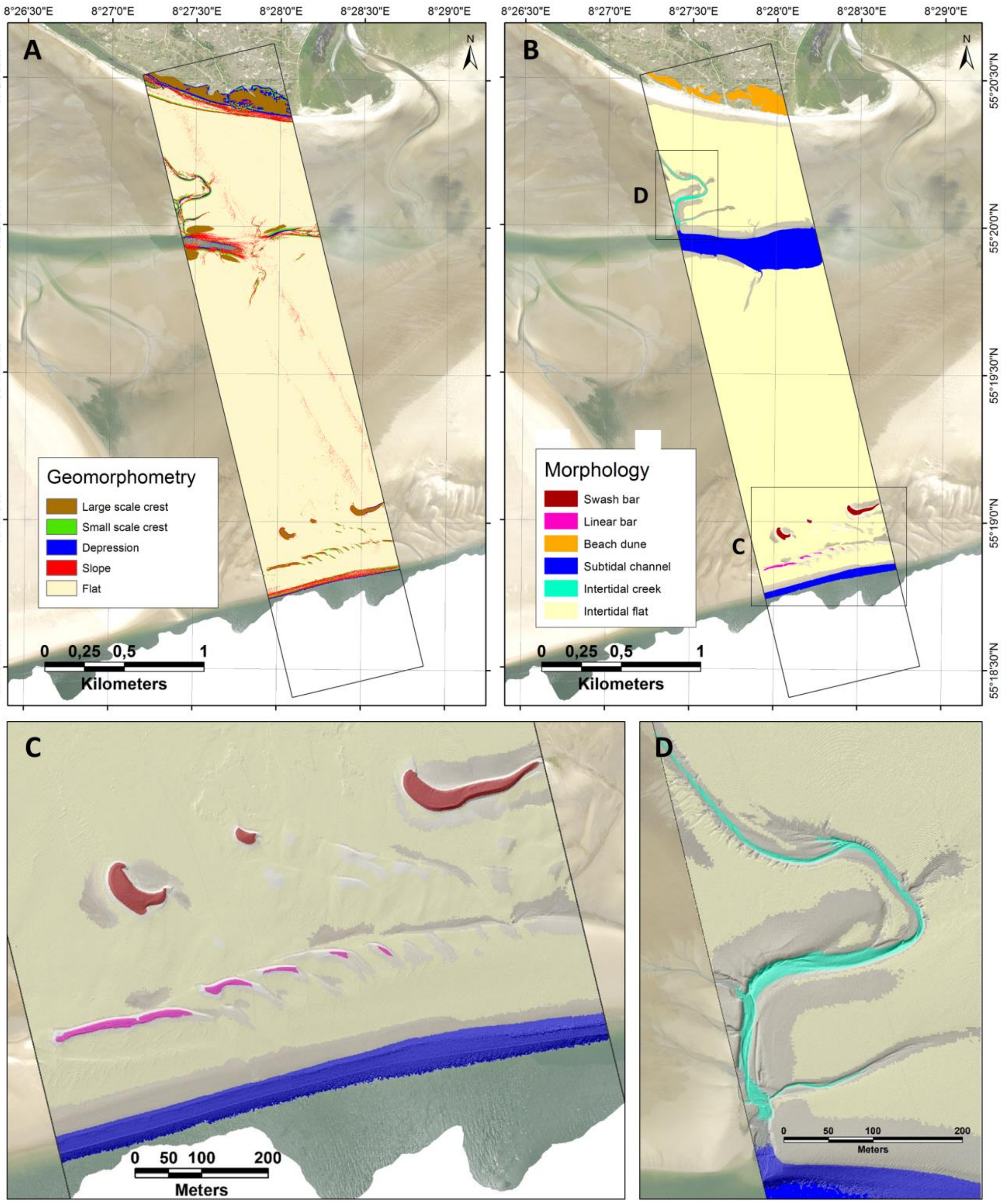

8°26'30"E
8°27'0"E
8°27'30"E
8°28'0"E
8°28'30"E
8°29'0"E
55°20'30"N
55°20'0"N
55°19'30"N
55°19'0"N
55°18'30"N
A
B
C
D
N
Geomorphometry
Large scale crest
Small scale crest
Depression
Slope
Flat
Morphology
Swash bar
Linear bar
Beach dune
Subtidal channel
Intertidal creek
Intertidal flat
0 0,25 0,5 1
Kilometers
0 50 100 200
Meters

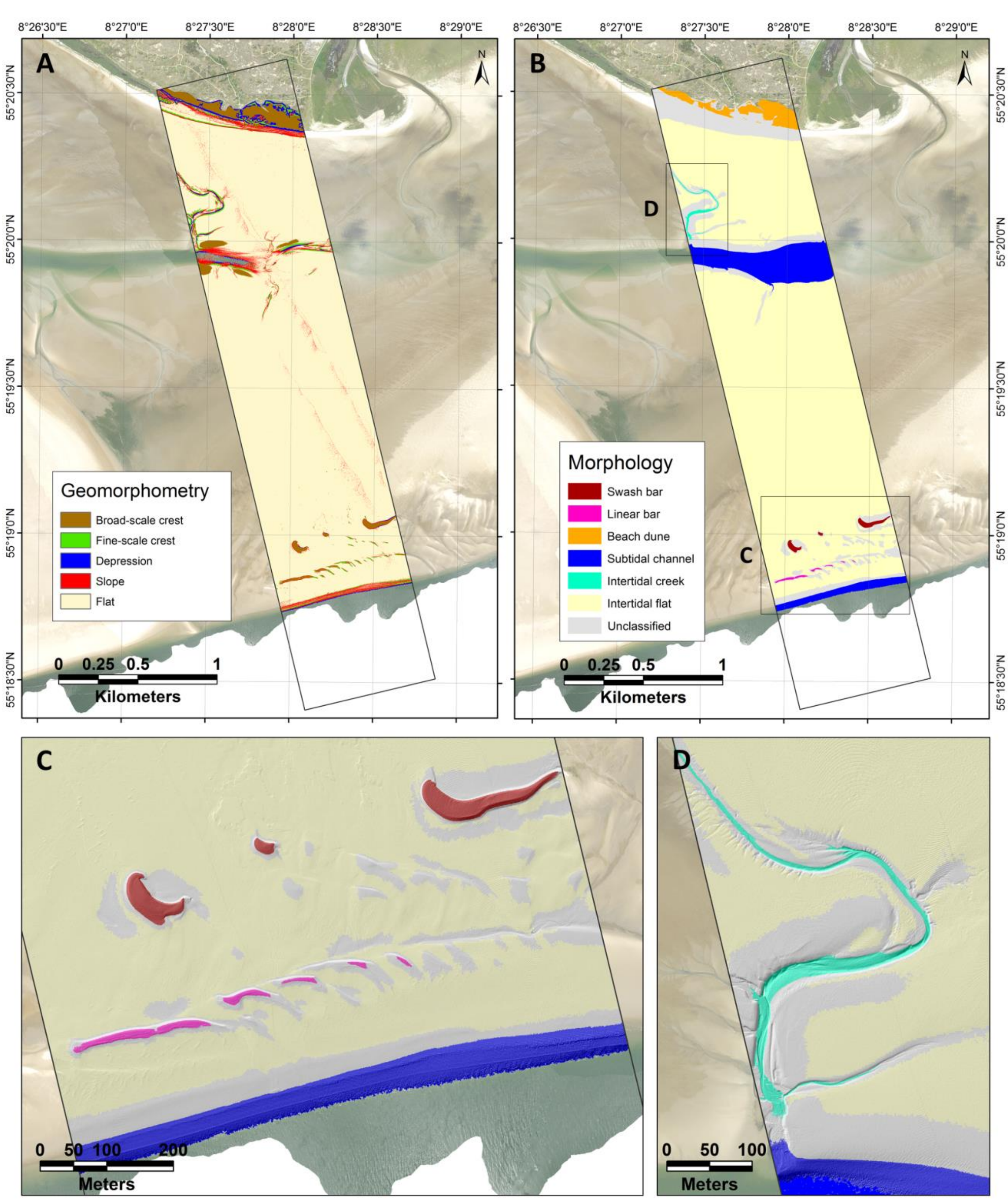

Figure 10: Two classifications ~~of the investigated section in Knudedyb tidal inlet system, ~~derived from ~~a ~~topobathymetric ~~DEM.~~LiDAR data: A) Geomorphometric classification~~.~~, and B) ~~morphological~~Morphological classification. C~~) Zoom in on the intertidal creek in the morphological classification. D~~) Zoom-in on the swash bars and linear bars close to the main channel in the morphological classification. D) Zoom-in on the intertidal creek in the morphological classification. A hillshade of the DEM is draped over C and D.

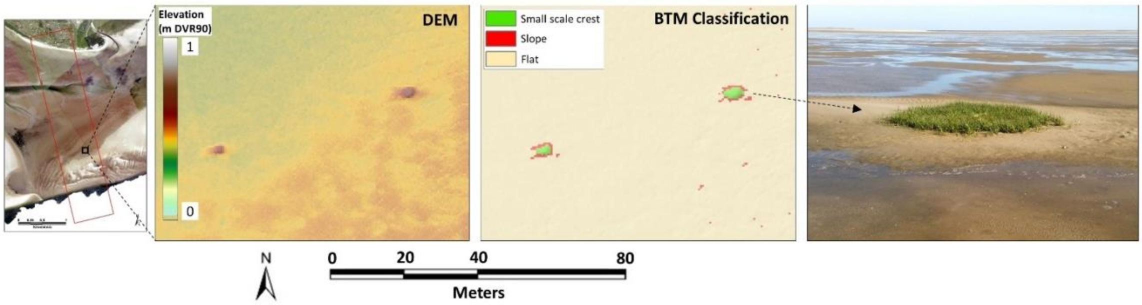

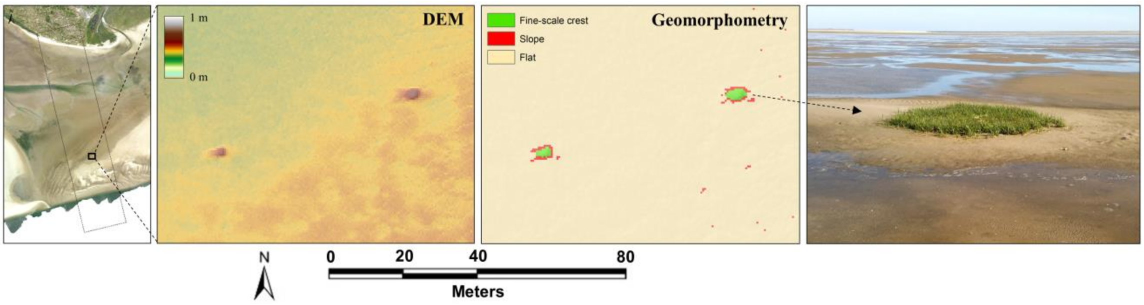

Figure 11: Vegetated mounds on the intertidal flat are clearly visible in the DEM and classified as ~~small~~fine-scale crests in the geomorphometric ~~BTM~~ classification. To the right is an image of one of the ~~patches~~mounds.

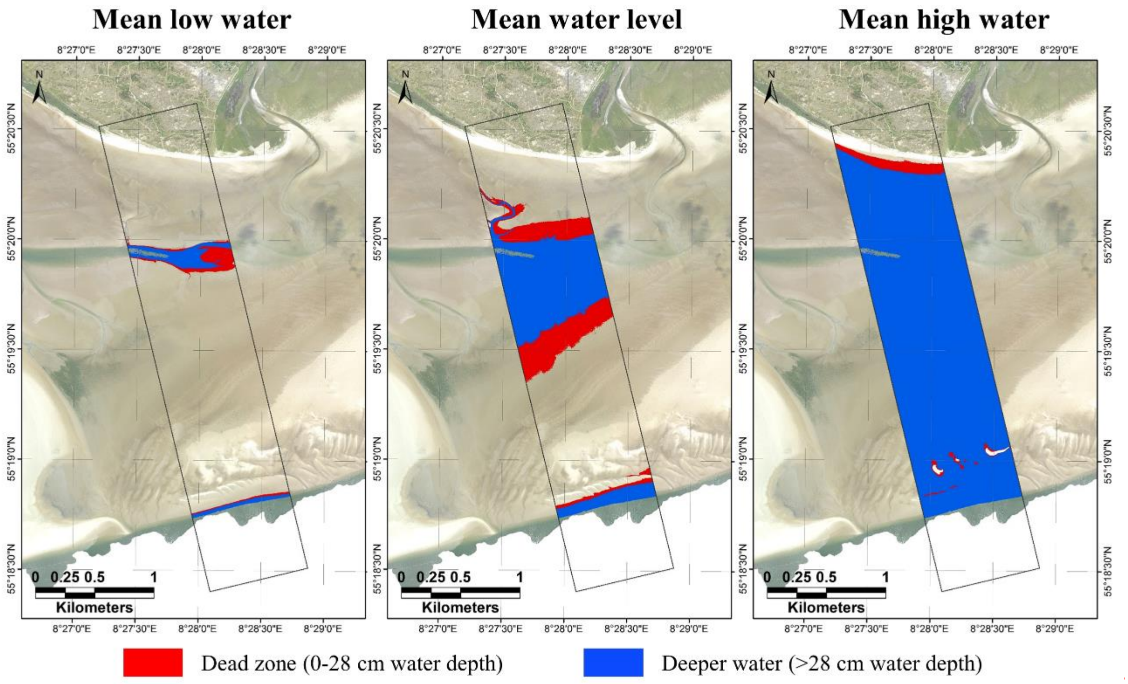
Mean low water
Mean water level
Mean high water
8°27'0"E
8°27'30"E
8°28'0"E
8°28'30"E
8°29'0"E
55°20'30"N
55°20'0"N
55°19'30"N
55°19'0"N
55°18'30"N
N
0 0.25 0.5 1
Kilometers
Dead zone (0-28 cm water depth)
Deeper water (>28 cm water depth)

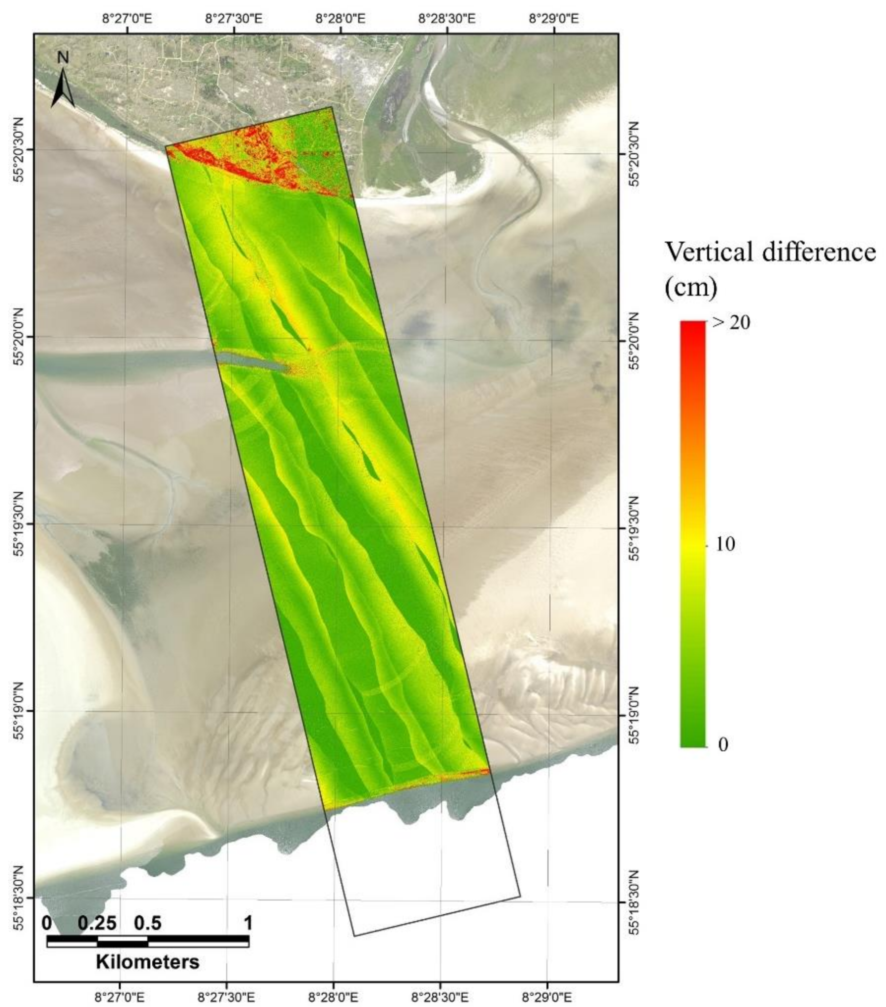

Figure 123: Vertical difference between the highest and the lowest LiDAR point within 0.5 × 0.5 m grid cells.